Journal of
Mechanics of
Materials and Structures

PERIDYNAMIC ANALYSIS OF FIBER-REINFORCED COMPOSITE MATERIALS

Erkan Oterkus and Erdogan Madenci

Volume 7, No. 1 January 2012

mathematical sciences publishers

JOURNAL OF MECHANICS OF MATERIALS AND STRUCTURES
Vol. 7, No. 1, 2012

msp

PERIDYNAMIC ANALYSIS OF FIBER-REINFORCED COMPOSITE MATERIALS

ERKAN OTERKUS AND ERDOGAN MADENCI

Damage growth in composites involves complex and progressive failure modes. Current computational tools are incapable of predicting failure in composite materials mainly due to their mathematical structure. However, peridynamic theory removes these obstacles by taking into account nonlocal interactions between material points. This study presents an application of peridynamic theory to predict how damage propagates in fiber-reinforced composite materials subjected to mechanical and thermal loading conditions.

1. Introduction

Damage initiation and its subsequent propagation in fiber-reinforced composites are not understood as clearly as they are, for example, for metals because of the presence of stiff fibers embedded into the soft matrix material, causing inhomogeneity. Under the assumption of homogeneity, a lamina has orthotropic elastic properties. Even though this assumption is suitable for stress analysis, it becomes questionable when predicting failure. Most composite structures include notches and cutouts, not only reducing the strength of the composites but also serving as potential failure sites for damage initiation. They also promote common failure modes of delamination, matrix cracking, and fiber breakage. These failure modes are inherent to the inhomogeneous nature of the composite, thus the homogeneous material assumption taints failure analyses.

In order to better understand failure mechanisms, Hallett and Wisnom [2006] conducted experiments on double-edge-notched composite specimens made from E-glass. They reported the occurrence of matrix cracking before ultimate failure for all specimens, representing four different layups when loaded in tension. Furthermore, it was reported that fiber failure initiated at the notch tip. Later, Green et al. [2007] investigated the effect of scaling on the tensile strength of notched composites made from unidirectional carbon-fiber/epoxy pre-preg by considering the hole diameter and laminate thickness as independent variables. These experiments showed that failure mechanisms in composites are very complex due to matrix cracking, fiber breakage, and delamination.

In order to investigate the behavior of cracks, Wu [1968] considered unidirectional fiberglass-reinforced Scotch-plies with center cracks oriented in the direction of the fibers. The plies had fibers in the 0° and 45° directions and were loaded in tension, pure shear, and combined tension and shear. In all three types of loading, it was observed that the crack propagated in a direction colinear with the initial crack.

It is, therefore, evident that the inhomogeneous nature of the composites must be retained in the analysis to predict the correct failure modes. Each lamina with a different fiber orientation must be modeled with distinct matrix and fiber properties.

Keywords: peridynamics, damage, nonlocal, composite.

Numerical studies on the failure of notched composites have mostly utilized the finite element method (FEM) to investigate the damage path and the initial failure load; such recent studies include [Bogert et al. 2006; Satyanarayana et al. 2007]. They predicted fiber and matrix damage in center-notched laminates for different layups under tension. Both the experimental observations and numerical results suggest that damage initiation and crack propagation are dependent on ply orientation.

Despite the development of many important concepts for predicting material behavior and failure, the prediction of failure modes and residual strengths of composite materials is a challenge within the framework of FEM. The use of FEM to predict failure can be quite challenging because remeshing may be required to make an accurate prediction and damage can only propagate in certain directions. Remeshing can be avoided by employing special elements, such as cohesive elements. However, these elements require a priori knowledge of the damage path, which might not be available. Unless these elements are correctly placed during model generation, the damage predictions may be erroneous. In addition to the need to remesh, existing methods for fracture modeling also suffer from the requirement of an external crack-growth criterion. This criterion prescribes how damage evolves a priori based on local conditions, and guides the analysis as to when and how damage initiates and propagates. Considering the difficulty in obtaining and generalizing experimental fracture data, providing such a criterion for damage growth, especially in composite structures, clearly presents a major obstacle to fracture modeling using conventional methods. This prevents such methods from being applicable to problems in which multiple damage growth occurs and interacts in complex patterns.

The difficulty in predicting failure using concepts from fracture mechanics in conjunction with FEM comes from the mathematical form of the classical continuum mechanics equations. The equations of motion in classical continuum mechanics are in the form of partial differential equations that involve the spatial displacement derivatives; however, these derivatives are undefined when the displacements are discontinuous, such as across cracks or interfaces. Hence, failure prediction is posterior and requires special techniques.

Silling [2000], realizing the aforementioned limitation, reintroduced a nonlocal theory that does not require spatial derivatives — the bond-based peridynamic (PD) theory. This theory accounts for only pairwise interaction between material points, thus resulting in the reduction of independent material constants. In order to remove this reduction, Silling et al. [2007] generalized bond-based PD theory by including the interaction of many material points. Referred to as state-based PD theory, it accounts for deviatoric and volumetric deformations, thus enforcing plastic incompressibility. The main difference between PD theory and classical continuum mechanics is that the former is formulated using integral equations as opposed to derivatives of the displacement components. This feature allows damage initiation and propagation at multiple sites with arbitrary paths inside the material without resorting to special crack-growth criteria. In PD theory, internal forces are expressed through nonlocal interactions between pairs of material points within a continuous body, and damage is a part of the constitutive model. Interfaces between dissimilar materials have their own properties, and damage can propagate when and where it is energetically favorable for it to do so.

PD theory was applied successfully in [Colavito et al. 2007a; 2007b] to predict damage in laminated composites subjected to low-velocity impact and static indentation. Askari et al. [2006] and Xu et al. [2007; 2008] also used PD simulations to predict damage in laminates subjected to low-velocity impact and in notched laminated composites under biaxial loads. Recently, Kilic et al. [2009] predicted the

basic failure modes of fiber, matrix, and delamination in various laminates with a preexisting central crack under tension. Also, Oterkus et al. [2010] demonstrated that PD analysis is capable of capturing bearing and shear-out failure modes in bolted composite lap-joints.

This study presents an application of PD theory in the analysis of fiber-reinforced composite materials subjected to mechanical and thermal loading conditions. The PD approach to modeling a lamina is first verified against analytical solutions within the realm of classical continuum mechanics by considering uniaxial tension and uniform temperature change. Then, damage growth patterns from a preexisting crack in a lamina for different fiber orientations are computed and compared with experimental observations. This approach is further extended to analyze composite laminates and to predict damage growth patterns from a preexisting crack in two distinct laminate constructions under tension. In the absence of a crack, the PD displacement predictions are compared with those of the classical laminate theory. In the presence of a crack, damage patterns are qualitative compared with experimental observations.

2. Peridynamic theory

The deformation response of solid structures subjected to external forces can be obtained by assuming the structure as a continuous body or a continuum, without paying attention to its atomistic structure. Hence, it is possible to perform both static and dynamic analyses of large structures within a reasonable amount of time. The conventional approach that is used to analyze solid structures is known as "classical continuum mechanics" and has been successfully applied to numerous problems in the past. Within the classical continuum mechanics framework, it is assumed that the continuous body is composed of an infinite number of infinitesimal volumes, which are called material points. These material points interact with each other only if they are within the nearest neighborhood of each other; in other words, through a direct interaction (contact). These interactions are expressed in terms of contact forces or tractions, $\boldsymbol{T}$, as shown in Figure 1.

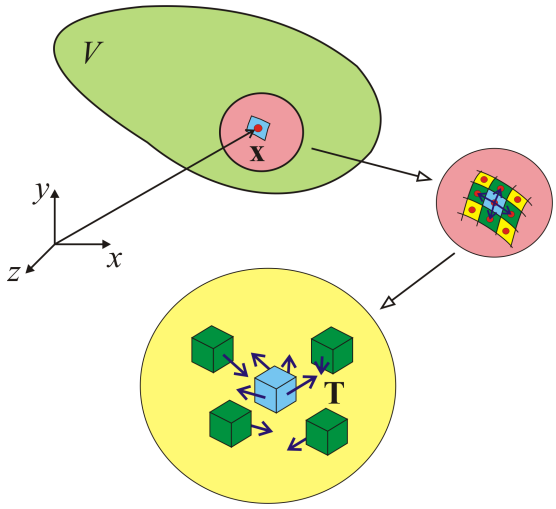

Figure 1. Interaction of material points in classical continuum mechanics.

Using the conservation of linear momentum and relating the traction vectors, $\boldsymbol{T}$, to the well-known stress tensor, $\boldsymbol{\sigma}$, results in the equation of motion of the material point, $\boldsymbol{x}$, in classical continuum mechanics:

$$\rho(\boldsymbol{x})\ddot{\boldsymbol{u}}(\boldsymbol{x},t) = \nabla\cdot\boldsymbol{\sigma} + \boldsymbol{b}(\boldsymbol{x},t), \tag{1}$$

where $\rho(\boldsymbol{x})$, $\boldsymbol{b}(\boldsymbol{x},t)$, and $\ddot{\boldsymbol{u}}(\boldsymbol{x},t)$ represent the mass density, body force density, and acceleration, respectively, of the material point located at $\boldsymbol{x}$. The spatial derivatives in the divergence operation associated with the stress tensor, $\boldsymbol{\sigma}$, do not exist on the discontinuity in the structure. Therefore, (1) is not valid for problems including discontinuities, such as cracks. Silling [2000] replaced the divergence term in (1) with an integral term, which makes the new form of the equation of motion applicable whether or not a discontinuity exists in the structure:

$$\rho(\boldsymbol{x})\ddot{\boldsymbol{u}}(\boldsymbol{x},t) = \int_H \boldsymbol{f}(\boldsymbol{x}'-\boldsymbol{x},\boldsymbol{u}'-\boldsymbol{u})\,dH + \boldsymbol{b}(\boldsymbol{x},t). \tag{2}$$

In (2), the domain of integration (neighborhood), H, includes all the material points that the material point $\boldsymbol{x}$ can interact with inside the body. The radius of the spherical neighborhood is referred to as the horizon, and it is denoted by δ. The interaction force or PD force between material points $\boldsymbol{x}$ and $\boldsymbol{x}'$ can be expressed as $\boldsymbol{f}(\boldsymbol{x}'-\boldsymbol{x},\boldsymbol{u}'-\boldsymbol{u})$, and it is a function of the relative position vector, $\boldsymbol{x}'-\boldsymbol{x}$, and relative displacement vector, $\boldsymbol{u}'-\boldsymbol{u}$. The PD force is along the same direction of the relative position of these material points in the deformed configuration, that is, $\boldsymbol{y}'-\boldsymbol{y} = (\boldsymbol{x}'+\boldsymbol{u}')-(\boldsymbol{x}+\boldsymbol{u})$. For an elastic isotropic material, the PD force takes the form

$$\boldsymbol{f} = c(s-s^*)\frac{\boldsymbol{y}'-\boldsymbol{y}}{|\boldsymbol{y}'-\boldsymbol{y}|} = c\bar{s}\frac{\boldsymbol{y}'-\boldsymbol{y}}{|\boldsymbol{y}'-\boldsymbol{y}|}, \tag{3}$$

where c, s, $\bar{s}$ and s^* represent the PD material parameter, total stretch, mechanical stretch, and thermal stretch between material points $\boldsymbol{x}$ and $\boldsymbol{x}'$, respectively. The total stretch, s, and the thermal stretch due to thermal loading, s^*, are defined as

$$s = \frac{|\boldsymbol{y}'-\boldsymbol{y}| - |\boldsymbol{x}'-\boldsymbol{x}|}{|\boldsymbol{x}'-\boldsymbol{x}|} \tag{4a}$$

and

$$s^* = \alpha\Delta T, \tag{4b}$$

where α and ΔT represent the coefficient of thermal expansion of the material and the temperature change, respectively. By using (4a) and (4b), the mechanical stretch, $\bar{s}$, can be computed as

$$\bar{s} = s - s^* = \frac{|\boldsymbol{y}'-\boldsymbol{y}| - |\boldsymbol{x}'-\boldsymbol{x}|}{|\boldsymbol{x}'-\boldsymbol{x}|} - \alpha\Delta T. \tag{5}$$

This form of the PD force representation, given in (3), accounts for pairwise interaction only between the material points. Therefore, it is limited to one independent material constant, c, with a Poisson's ratio of $\frac{1}{4}$ and $\frac{1}{3}$ in three- and two-dimensional analysis, respectively. This material parameter, c, can be related to the engineering material constants by equating the strain energy densities of the PD and

classical continuum theories at a material point inside a body due to simple loading, such as uniform expansion. Silling and Askari [2005] derived an explicit expression for parameter c in the form

$$c = \frac{18\kappa}{\pi\delta^4}, \tag{6}$$

where κ is the bulk modulus of the material and δ represents the radius of a spherical horizon.

Based on PD theory, the strain energy density of a material point at $\boldsymbol{x}$, U_{PD}, can be expressed as

$$U_{\mathrm{PD}} = \frac{1}{2}\int_H w\, dH, \tag{7}$$

where the micropotential, w, is defined as

$$w = \tfrac{1}{2}c(s - s^*)^2\xi = \tfrac{1}{2}c\bar{s}^2\xi, \tag{8a}$$

with

$$\xi = |\boldsymbol{x}' - \boldsymbol{x}|. \tag{8b}$$

It can also be assumed that two material points, $\boldsymbol{x}$ and $\boldsymbol{x}'$, cease to interact with each other if the mechanical stretch between these material points exceeds a critical stretch value, s_0, as shown in Figure 2. This material model represents an elastic material behavior without allowing any permanent deformation.

Termination of the interaction between material points can be associated with the failure of the material by modifying the PD force relation given in (3) by introducing the failure parameter $\mu(\boldsymbol{x}' - \boldsymbol{x}, t)$

$$\boldsymbol{f} = \mu(\boldsymbol{x}' - \boldsymbol{x}, t)c(s - s^*)\frac{\boldsymbol{y}' - \boldsymbol{y}}{|\boldsymbol{y}' - \boldsymbol{y}|}, \tag{9}$$

where the failure parameter can be defined as

$$\mu(\boldsymbol{x}' - \boldsymbol{x}, t) = \begin{cases} 1 & \text{if } s(\boldsymbol{x}' - \boldsymbol{x}, t') - s^* < s_0 \text{ for all } 0 < t' < t, \\ 0 & \text{otherwise.} \end{cases} \tag{10}$$

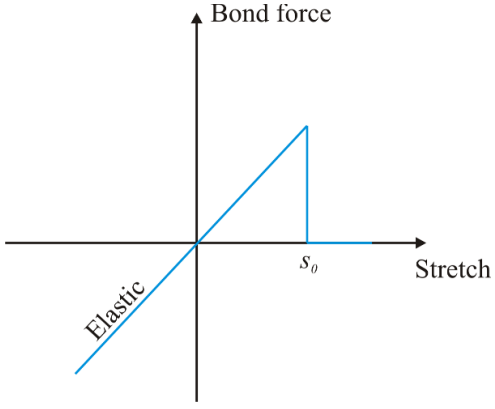

Figure 2. Constitutive relation between material points in an elastic material.

The inexplicit nature of local damage at a material point, $\boldsymbol{x}$, arising from the introduction of failure in the constitutive model, is removed by defining the local damage as

$$\varphi(\boldsymbol{x}, t) = 1 - \frac{\int_H \mu(\boldsymbol{x}' - \boldsymbol{x}, t)\, dH}{\int_H dH}. \tag{11}$$

Thus, local damage is the weighted ratio of the number of the broken interactions to the total number of interactions within the horizon, H. The extent of damage is defined by a value between 0 and 1, where 0 indicates that a material point has no damage and 1 indicates complete damage at the material point. Also, a damage value of 0.5 and above indicates possible cracking.

In the case of isotropic materials, value s_0 of the critical stretch can be related to the equivalent energy release rate as derived in [Silling and Askari 2005]:

$$s_0 = \sqrt{\frac{5G_0}{9\kappa\delta}}, \tag{12}$$

where G_0 is the critical energy release rate of the material and can be related to the fracture toughness of the material.

In order to solve (2), a collocation method is adopted and the numerical treatment involves the discretization of the domain of interest into subdomains. The domain can be discretized into cubic subdomains. With this discretization, the volume integration in (2) is approximated, leading to

$$\rho(\boldsymbol{x}_{(i)})\ddot{\boldsymbol{u}}(\boldsymbol{x}_{(i)}, t) = \sum_{j=1}^{M} \boldsymbol{f}\big(\boldsymbol{u}(\boldsymbol{x}_{(j)}, t) - \boldsymbol{u}(\boldsymbol{x}_{(i)}, t), \boldsymbol{x}_{(j)} - \boldsymbol{x}_{(i)}\big) V_{(j)} + b(\boldsymbol{x}_{(i)}, t), \tag{13}$$

where $\boldsymbol{x}_{(i)}$ is the position vector located at the i-th collocation (material) point and M is the number of subdomains within the horizon of the i-th material point. The position vector $\boldsymbol{x}_{(j)}$ represents the location of the j-th collocation point. The volume of the j-th subdomain is $V_{(j)}$.

Since peridynamics is a nonlocal theory and its equations of motion utilize integrodifferential equations as opposed to partial differential equations in the case of the classical continuum theory, the application of boundary conditions is different from that of the classical continuum theory. The tractions or point forces cannot be applied as boundary conditions since their volume integrations result in a zero value [Oterkus and Madenci 2012]. Therefore, the boundary conditions are applied over the volumes as body forces, displacements, and velocities. As explained in [Macek and Silling 2007], the thickness of the region over which the boundary conditions are applied should be comparable to the size of the horizon.

3. Peridynamic analysis of a lamina

If a fiber-reinforced composite lamina is considered, the directional dependency must be included in the PD analysis. Therefore, two different PD material parameters are introduced as shown in Figure 3 to model a fiber-reinforced composite lamina with a fiber orientation of θ. The material point q represents material points that interact with material point i only along the fiber direction. However, the material point p represents material points that interact with material point i in any direction, including the fiber

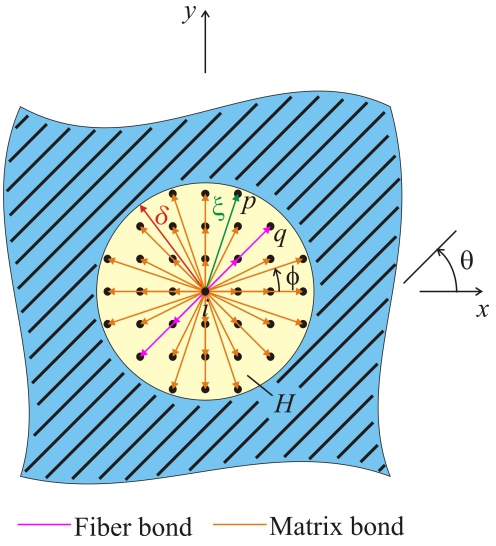

Figure 3. PD horizon for a lamina with a fiber orientation of θ and PD bonds between material point i and other material points within its horizon.

direction. The orientation of a PD bond between the material point i and the material point p is defined by the angle ϕ with respect to the x-axis.

Associated with a lamina, the material parameter concerning the interaction of material points only in the fiber direction is denoted by c_f. The interaction of material points in all other directions within a lamina is governed by the material parameter, c_m. Extending the procedure introduced in [Gerstle et al. 2005] for isotropic materials, the PD material parameters, c_f and c_m, can be expressed analytically in terms of the engineering material constants, E_1, E_2, G_{12}, and ν_{12}, by equating strain energy densities of a material point based on the classical continuum mechanics and PD theory for simple loading conditions.

The constitutive or force-stretch relations for the in-plane interactions of two material points, referred to as fiber and matrix bonds, are shown in Figure 4. The critical parameters that define the failure of these

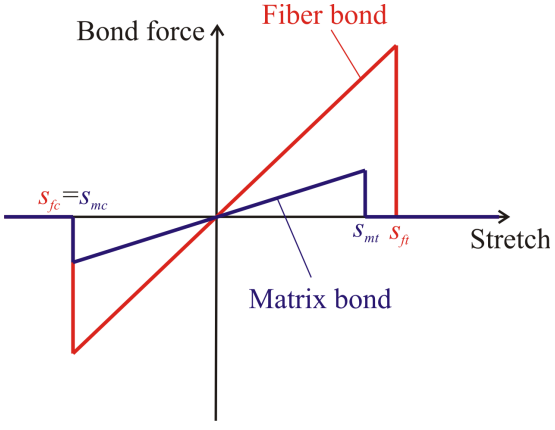

Figure 4. Force-stretch relation for fiber and matrix bonds.

bonds under tension and compressions are $(s_{\text{ft}}, s_{\text{mt}})$ and $(s_{\text{fc}}, s_{\text{mc}})$, respectively, and can be determined based on the experimental measurements. Determination of these critical stretch parameters are explained in Oterkus et al. [2012].

Based on the classical continuum mechanics, the strain energy density of a material point, U_{CCM}, for a two-dimensional composite lamina is expressed as

$$U_{\text{CCM}} = \tfrac{1}{2}\boldsymbol{\sigma}^T(\boldsymbol{\epsilon} - \boldsymbol{\epsilon}^*), \tag{14}$$

in which the stress, $\boldsymbol{\sigma}$, total strain, $\boldsymbol{\epsilon}$, and thermal strain vectors, $\boldsymbol{\epsilon}^*$, are defined as

$$\boldsymbol{\sigma}^T = \left\{\sigma_{xx} \;\; \sigma_{yy} \;\; \tau_{xy}\right\}, \qquad \boldsymbol{\epsilon}^T = \left\{\epsilon_{xx} \;\; \epsilon_{yy} \;\; \gamma_{xy}\right\}, \qquad \boldsymbol{\epsilon}^{*T} = \left\{\epsilon^*_{xx} \;\; \epsilon^*_{yy} \;\; \gamma_{xy}\right\}. \tag{15}$$

For a composite lamina with a fiber orientation of θ, the stress and strain components are related through the constitutive relation as

$$\boldsymbol{\sigma} = \overline{\boldsymbol{Q}}(\boldsymbol{\epsilon} - \boldsymbol{\epsilon}^*), \tag{16}$$

where the transformed reduced stiffness matrix $\overline{\boldsymbol{Q}}$ is defined as

$$\overline{\boldsymbol{Q}} = \begin{bmatrix} \overline{Q}_{11} & \overline{Q}_{12} & \overline{Q}_{16} \\ \overline{Q}_{12} & \overline{Q}_{22} & \overline{Q}_{26} \\ \overline{Q}_{16} & \overline{Q}_{26} & \overline{Q}_{66} \end{bmatrix}. \tag{17}$$

The transformed reduced stiffness matrix, $\overline{\boldsymbol{Q}}$ is a function of four independent material constants of elastic modulus in the fiber direction, E_1, elastic modulus in the transverse direction, E_2, in-plane shear modulus, G_{12}, and in-plane Poisson's ratio, ν_{12}. The explicit expressions for the components of $\overline{\boldsymbol{Q}}$ can be found in any textbook on mechanics of composite materials — for example, [Kaw 2006]. The thermal expansion coefficients in the fiber and transverse directions are specified as α_1 and α_2, respectively.

Alternatively, the strain energy density of the same material point in PD theory, U_{PD}, can be calculated using (7). However, the material parameter, c has a directional dependency of the form

$$c = \begin{cases} c_f + c_m & \text{for } \phi = \theta, \\ c_m & \text{for } \phi \neq \theta. \end{cases} \tag{18}$$

Therefore, (8a) for the micropotential should be modified as

$$w = \tfrac{1}{2}c(\phi)\bar{s}^2(\phi)\xi(\phi), \tag{19}$$

in which ϕ represents the bond angle. With this representation, the integration in (7) for the strain energy density of material point i shown in Figure 3 cannot be fully performed analytically. However, it can be approximated as

$$U_{\text{PD}} = \frac{1}{2}\sum_{q=1}^{Q}\frac{c_f s_{qi}^2 \xi_{qi}}{2}V_q + \frac{1}{2}\int_H \frac{c_m s^2 \xi}{2}\,dH, \tag{20}$$

in which Q is the number of fiber bonds within its horizon, δ. As apparent in this equation, the fiber bond constant, c_f depends on the discretization, whereas the matrix bond constant, c_m, does not because it does not have a directional property unlike the fibers. The initial length of the bond in the fiber direction and its stretch after deformation between material points q and i are denoted by ξ_{qi} and s_{qi}, respectively.

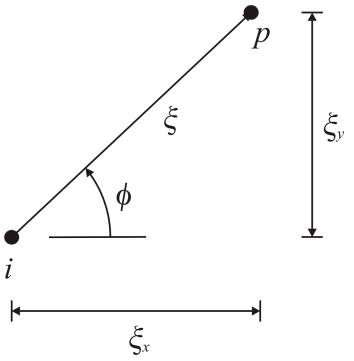

Figure 5. Components of the initial bond length between material points i and p.

The volume of the material point q that interacts with material point i is denoted by V_q, which can be approximated as

$$V_q = \frac{\pi t \delta^2}{N}, \tag{21}$$

in which N is the number of material points within its horizon, δ, and t is the thickness of the lamina.

The initial length and stretch of the bond between the material points i and p are referenced to a polar coordinate system (ξ, ϕ). As shown in Figure 5, the components of the initial bond length, ξ, in the x- and y-directions are denoted by ξ_x and ξ_y, respectively, and are given by

$$\xi_x = \xi \cos\phi, \qquad \xi_y = \xi \sin\phi. \tag{22}$$

The PD strain energy density of a material point i, given in (20), can be expressed in terms of bond constants c_f and c_m, representing the fiber and matrix, by identifying the direction of the bond

$$U_{\mathrm{PD}} = \beta_f c_f + \beta_m c_m. \tag{23}$$

The coefficients β_f and β_m in (23) can be determined by computing the stretch, s_{pi}, and the initial length, ξ_{pi}, of the bond between the material points i and p, and the volume of material point p, V_p.

In order to determine the bond constants c_f and c_m in terms of the engineering constants E_1, E_2, G_{12}, and ν_{12}, a uniaxial loading condition can be considered as explained in Appendix A. Equating the strain energy densities from PD theory and classical continuum mechanics for this loading condition results in explicit expressions for c_f and c_m,

$$c_f = \frac{2E_1(E_1 - E_2)}{(E_1 - \frac{1}{9}E_2)\sum_{q=1}^{Q} \xi_{qi} V_q}, \qquad c_m = \frac{8E_1E_2}{(E_1 - \frac{1}{9}E_2)\pi t \delta^3}, \tag{24}$$

along with constraints on material constants G_{12} and ν_{12},

$$G_{12} = \frac{\nu_{12}E_2}{1 - \nu_{21}\nu_{12}} = \frac{E_1E_2}{3(E_1 - \frac{1}{9}E_2)}, \qquad \nu_{12} = \frac{1}{3}. \tag{25}$$

As discussed in [Oterkus and Madenci 2012], because of the pairwise interaction of material points, four independent material constants of a lamina reduce to two independent constants. In the case of an isotropic material, the bond constant for fiber, c_f, given in $(24)_1$ becomes zero. This indicates that for

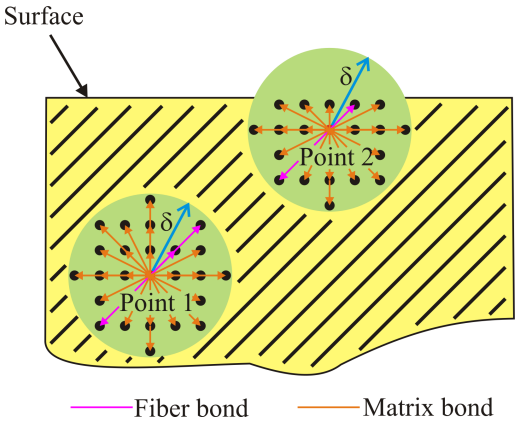

Figure 6. Surface effects in the domain of interest.

an isotropic material, the material should be described by using only one bond constant, c_m. In this case the expression for c_m in $(24)_2$ recovers the expression for an isotropic material, that is, $c_m = 9E/\pi t\delta^3$, given in [Oterkus and Madenci 2012].

In the case of thermal loading, the stretch is obtained by (4b), and the coefficient of thermal expansion, $\alpha(\phi)$, for a lamina is also dependent on the bond orientation between material points i and p. As derived in Appendix A, it can be expressed in terms of coefficients of thermal expansion for an angle lamina, α_x, α_y, and α_{xy}, in the form

$$\alpha(\phi) = \alpha_x \cos^2\phi + \alpha_y \sin^2\phi + \alpha_{xy} \sin\phi \cos\phi. \tag{26}$$

3.1. ***Surface correction factors for a lamina.*** Surface correction is an important concept in PD theory. The response function given in (3) is derived under the assumption that the material point located at $\boldsymbol{x}$ is in a single material with its complete neighborhood entirely embedded within its horizon, δ. However, this assumption becomes invalid when the material point is close to free surfaces (Figure 6). It results in a reduction in material stiffness near the free surfaces, and this stiffness reduction must be corrected. After determining the surface correction factor for each bond, the PD force in that bond is modified based on the associated surface correction factor. Determination of surface correction factors for isotropic materials is explained in detail by [Oterkus and Madenci 2012]. However, the determination of surface correction factors for a lamina is more complicated than that for an isotropic material because of two different PD bonds. Detailed derivations of the surface correction factors for fiber and matrix bonds are given in Appendix B.

4. Peridynamic analysis of a laminate

The PD formulation for a composite lamina can be extended to consider a composite laminate. In order to capture the deformation behavior of a laminate in the thickness direction and define the interaction between neighboring plies, two additional bond constants between neighboring plies are introduced, as shown in Figure 7.

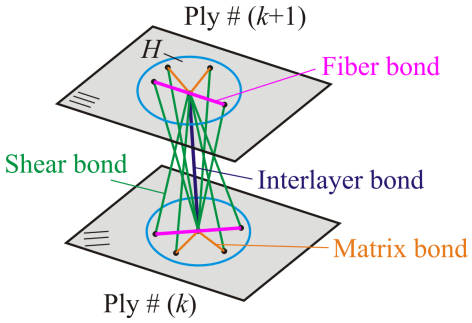

Figure 7. Four different bond constants for a fiber-reinforced composite material.

Similar to the approach implemented in the peridynamic code (Emu) developed in [Silling 2000], transverse normal and shear deformations between material points located on adjacent (neighboring) layers are related through the bond constants c_{in} and c_{is}, respectively. As shown in Figure 7, interlayer bonds only exist in the normal direction, whereas shear bonds exist in all directions between the neighboring plies. Hence, a material point can interact with two other material points via interlayer bonds that have the same in-plane coordinates.

As in the case of in-plane deformation of a lamina, the interlayer and shear bond constants, c_{in} and c_{is}, can be derived in the form

$$c_{in} = \frac{E_m}{t\overline{V}}, \qquad c_{is} = \frac{2G_m}{\pi t}\,\frac{1}{\delta^2 + t^2 \ln \dfrac{t^2}{\delta^2 + t^2}}, \tag{27}$$

where E_m and G_m are the elastic modulus and shear modulus of the matrix material, respectively, and $\overline{V}$ is the volume of a material point. Detailed derivations of these expressions are given in Appendix C.

Note that the shear bonds have a different characteristic than the fiber, matrix and interlayer bonds because the shear bond constant relates the body force density, $\boldsymbol{f}$, to the change in angle of the bond from its original orientation (shear angle), φ. Therefore, the force density and micropotential expressions for a shear bond can be written as

$$\boldsymbol{f} = c_s \varphi (\Delta x)^2 \frac{\boldsymbol{y}' - \boldsymbol{y}}{|\boldsymbol{y}' - \boldsymbol{y}|}, \qquad w = \tfrac{1}{2} c_s \varphi^2, \tag{28}$$

where Δx is the spacing between material points on the in-plane of the lamina.

Failure of the interlayer and shear bonds corresponds to mode I and mode II, respectively. Interlayer damage represents the breakage of (interlayer) bonds between a layer and its adjacent layers above and below. Hence, it provides the extent of delamination between the adjacent layers. Therefore, the interlayer bonds are assumed to fail only in tension. The critical stretch value for the interlayer bonds, s_{in}, can be obtained analytically by equating the energy consumed by an advancing mode-I crack to the work required to break all interlayer bonds as

$$s_{in} = \sqrt{\frac{2G_{IC}}{t E_m}}, \tag{29}$$

where G_{IC} is the mode-I critical energy release rate of the matrix material.

The shear bonds can fail if the shear angle of the bonds exceeds the critical shear angle value, φ_c. It can also be obtained analytically by equating the energy consumed by an advancing mode-II crack to the work required to break all shear bonds as

$$\varphi_c = \sqrt{\frac{G_{IIC}}{tG_m}}, \tag{30}$$

where G_{IIC} is the mode-II critical energy release rate of the matrix material.

Derivations of the relationships between the critical stretch value for the interlayer bonds, s_{in}, and the mode-I critical energy release rate and between the critical shear angle value, φ_c, and the mode-II critical energy release rate are given in Appendix D.

5. Numerical results

5.1. ***A lamina under uniaxial tension and uniform temperature change.*** A unidirectional thin lamina with a fiber orientation of $\theta = 0°$ is considered, as shown in Figure 8. The length and width of the lamina are specified as $L = 15.24$ mm and $W = 7.62$ mm, respectively. It has a thickness of $t = 0.1651$ mm. Its elastic moduli in the fiber and transverse directions are $E_1 = 159.96$ GPa and $E_2 = 8.96$ GPa, respectively. The thermal expansion coefficients in the fiber and transverse directions are $\alpha_1 = -1.52$ ppm/°C and $\alpha_2 = 34.3$ ppm/°C, respectively. The PD model is generated by using a single layer of material points with a grid size of $\Delta x = 6.35 \times 10^{-4}$ m. The horizon radius is specified as $\delta = 3.015\Delta x$. Using (24), the fiber and matrix bond constants are computed as $c_f = 5.72 \times 10^{23}$ N/m^6 and $c_m = 1.86 \times 10^{22}$ N/m^6. The quasistatic solution is obtained by using the adaptive dynamic relaxation technique by using a time increment of 1 and stable mass density value of 7.005×10^{18} kg/m^3 [Kilic 2008]. Failure is not allowed in order to verify the solution against analytical predictions based on classical continuum mechanics.

First, a uniaxial tension loading of $P = 159.96$ MPa is applied as a body load of $b_x = 5.95 \times 10^{10}$ N/m^3 along the edges of the lamina through a volumetric region with a depth of $b = 2.54 \times 10^{-3}$ m. The variation

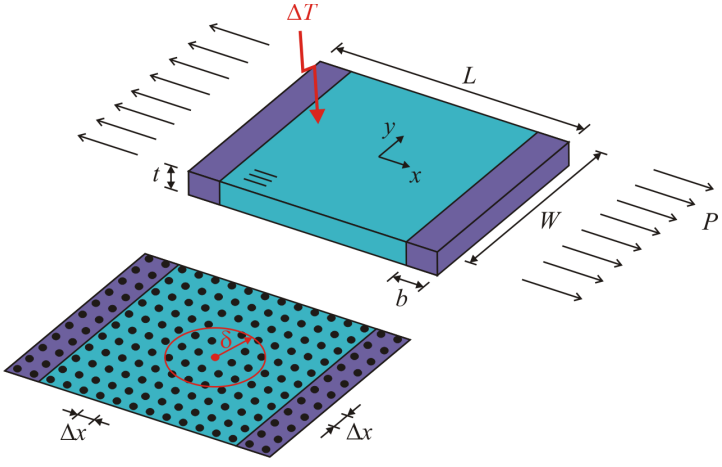

Figure 8. Loading and geometry of the unidirectional lamina under uniaxial tension and uniform temperature change.

of the horizontal and vertical displacement components along the central axes in the x- and y-directions, respectively, are computed at the end of 8000 time steps and compared with analytical results, as shown in Figures 9 and 10. Analytical results based on the classical continuum mechanics are computed by using the relations

$$u_x = \frac{P}{E_1}x, \qquad u_y = -\nu_{12}\frac{P}{E_1}y. \tag{31}$$

For both displacement components, there is remarkable agreement between the analytical and PD results.

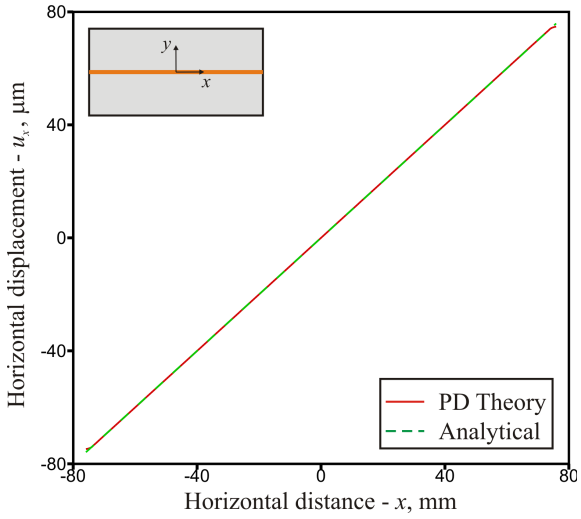

Figure 9. Horizontal displacement along the central axis at the end of 8000 time steps.

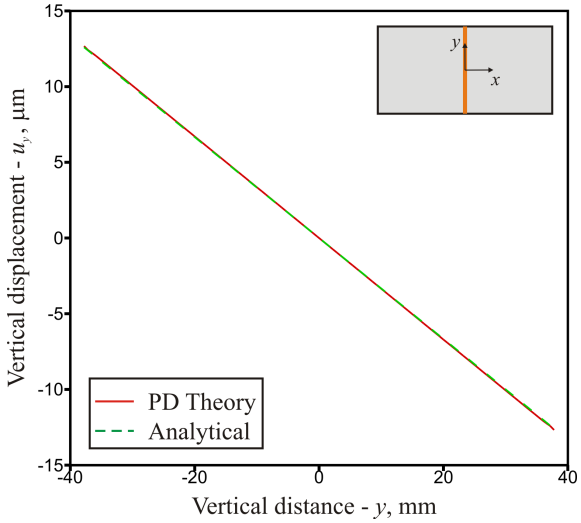

Figure 10. Vertical displacement along the central axis at the end of 8000 time steps.

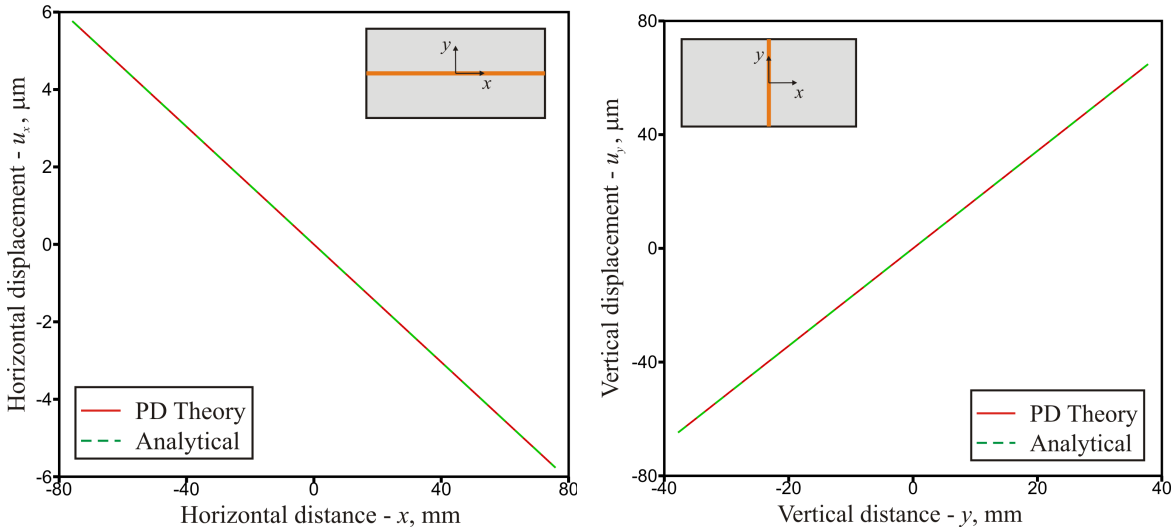

Figure 11. Variation of horizontal (left) and vertical (right) displacement along the central axis at the end of 8000 time steps when no failure is allowed.

Second, the lamina is only subjected to a uniform temperature change of $\Delta T = 50\,^{\circ}\mathrm{C}$. For this loading condition, the analytical horizontal and vertical displacements along the central axes are computed by

$$u_x = \alpha_1 \Delta T x, \qquad u_y = \alpha_2 \Delta T y. \tag{32}$$

Comparisons of horizontal and vertical displacements obtained analytically and from PD analysis, shown in Figure 11, indicate remarkably close agreement.

5.2. ***Laminates under uniaxial tension.*** The validation is continued by considering two different 3-ply laminates with stacking sequences of [0°/90°/0°] and [0°/45°/0°] subjected to uniform tension loading, as

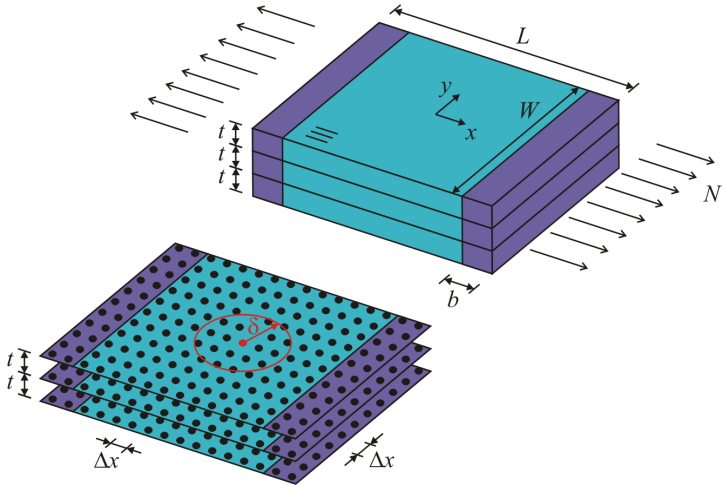

Figure 12. Loading and geometry of a composite laminate under uniaxial tension.

shown in Figure 12. The geometrical and material properties are the same as those of the lamina. Using (27), the interlayer and shear bond constants are computed as $c_{in} = 3.45 \times 10^{23}$ N/m^6 and $c_{is} = 1.55 \times 10^{18}$ N/m^5, respectively. The uniaxial tension loading is applied as a body load of $b_x = 5.95 \times 10^{10}$ N/m^3 through a volumetric region with a depth of $b = 2.54 \times 10^{-3}$ m. It corresponds to a stress resultant value of $N = 79228.2$ N/m along the edges of the laminate. During the solution, failure is not allowed in order to compare with the analytical solution based on the classical laminate theory.

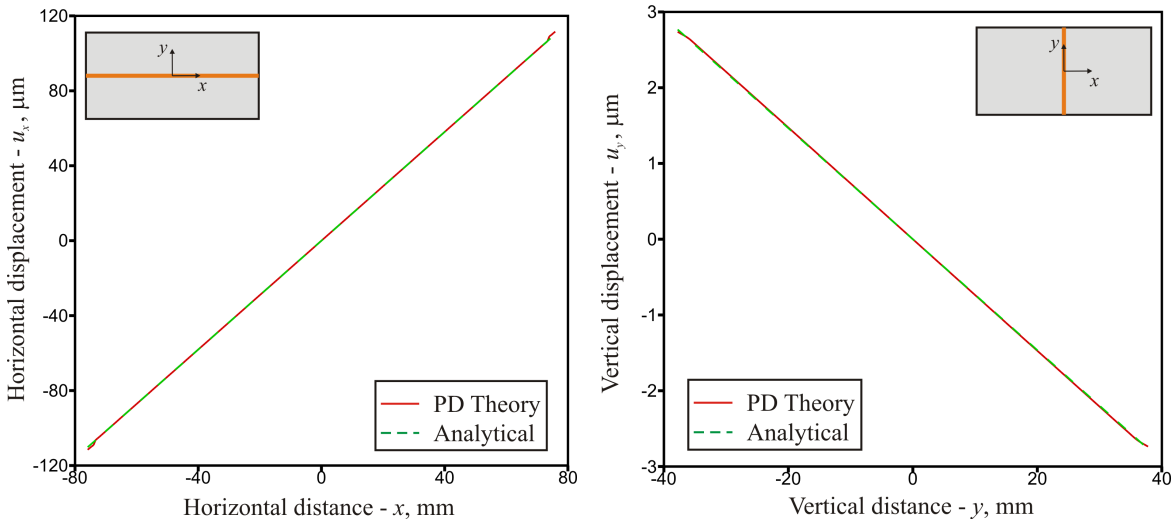

Figure 13. Horizontal (left) and vertical (right) displacement along the central axis in the 90° ply of the [0°/90°/0°] layup at the end of 8000 time steps.

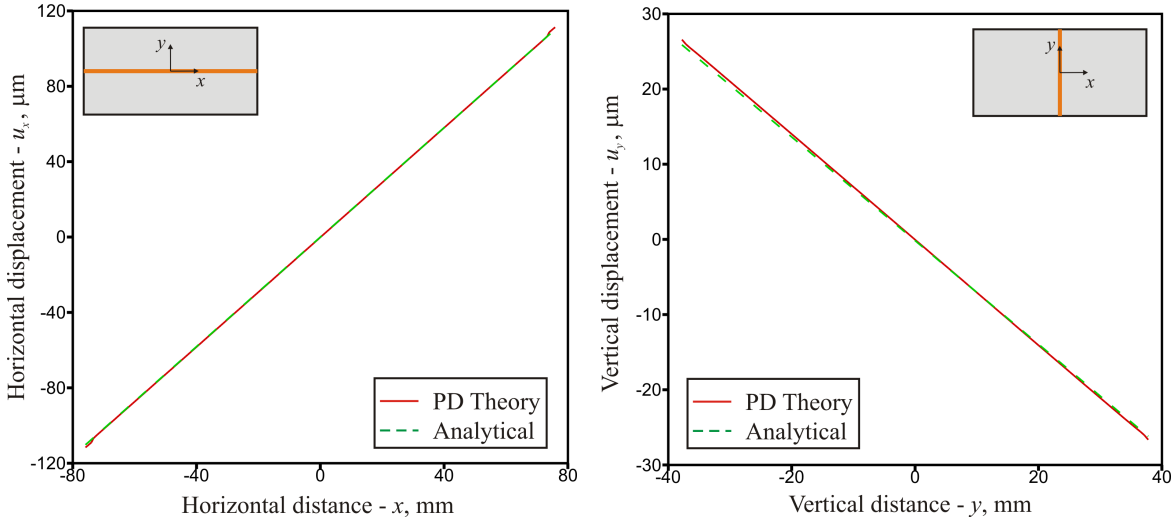

Figure 14. Horizontal (left) and vertical (right) displacement along the central axis in the 45° ply of the [0°/45°/0°] layup at the end of 8000 time steps.

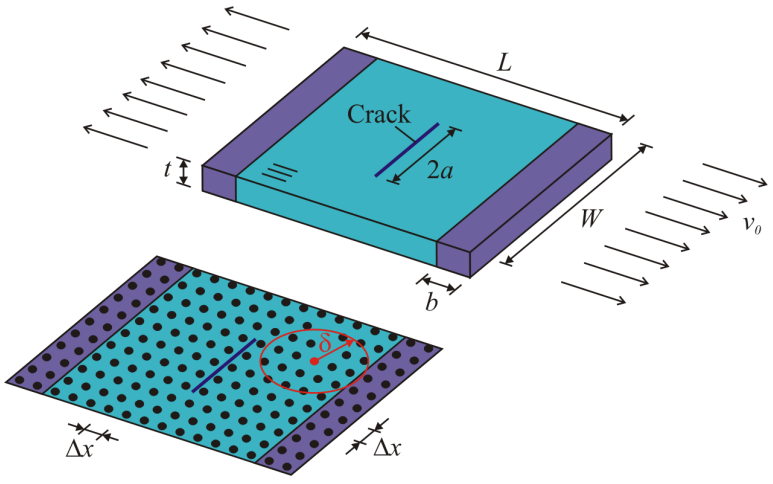

Figure 15. Loading and geometry of the unidirectional lamina with a crack under tension loading.

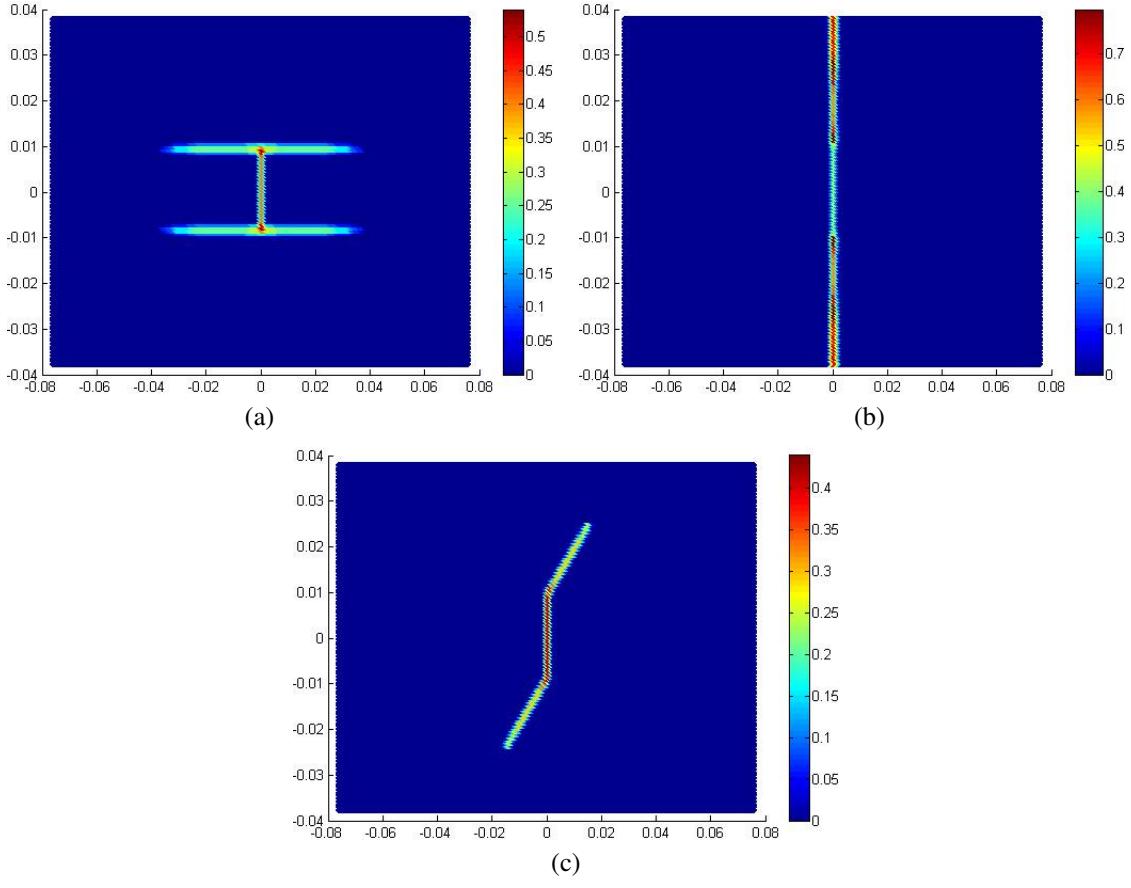

Figure 16. Damage plots for a lamina having a central crack with a fiber orientation of (a) $\theta = 0°$, (b) $\theta = 90°$, and (c) $\theta = 45°$.

The variation of the horizontal and vertical displacement components along the central axes in the x- and y-directions, respectively, for the 90° ply of the [0°/90°/0°] layup are computed at the end of 8000 time steps and compared with analytical results, as shown in Figure 13. The comparison of the displacement components in the 45° ply of the [0°/45°/0°] layup is shown in Figure 14. For both laminates, the agreement between the analytical and PD displacements is remarkably close.

5.3. ***A lamina with a preexisting central crack under tension.*** In order to demonstrate the failure prediction capability of the PD approach, the same lamina used previously, with a preexisting central crack, is considered for three different fiber orientations, $\theta = 0°$, 90°, and 45°. As shown in Figure 15, the crack is aligned with the y-axis and has a length of $2a = 0.01778$ m. The lamina is subjected to a velocity boundary condition of $v_0 = 2.02 \times 10^{-7}$ m/s along the edges of the lamina through a volumetric region with a depth of $b = 2.54 \times 10^{-3}$ m. Failure is only allowed in tension for the fiber and matrix bonds. The critical stretch for the matrix bond is specified as $s_{\text{mt}} = 0.0135$, which can be obtained by using the critical stretch expression given by (12) for an epoxy material. The procedure for computing this critical stretch value is demonstrated in Appendix D. For the fiber bond, it is assumed that its critical stretch value is twice the critical stretch for the matrix bond, that is, $s_{\text{ft}} = 0.027$.

As shown in Figure 16, in all cases the crack propagates in the fiber direction referred to as the splitting mode. Similar experimental observations confirm that current PD model accurately captures the failure modes.

5.4. ***Laminates with a preexisting central crack under tension.*** The failure prediction capability of the PD theory is further demonstrated by introducing a central crack in the two laminate layups of [0°/90°/0°] and [0°/45°/0°]. As shown in Figure 17, the crack is aligned with the y-axis and has a length of $2a = 0.01778$ m. The laminates are subjected to a velocity boundary condition of $v_0 = 2.02 \times 10^{-7}$ m/s. The critical stretch parameters specified for the fiber and matrix bonds are $s_{\text{ft}} = 0.027$ and $s_{\text{mt}} = 0.0135$, respectively. The critical stretch and angle parameters for the interlayer and shear bonds are computed

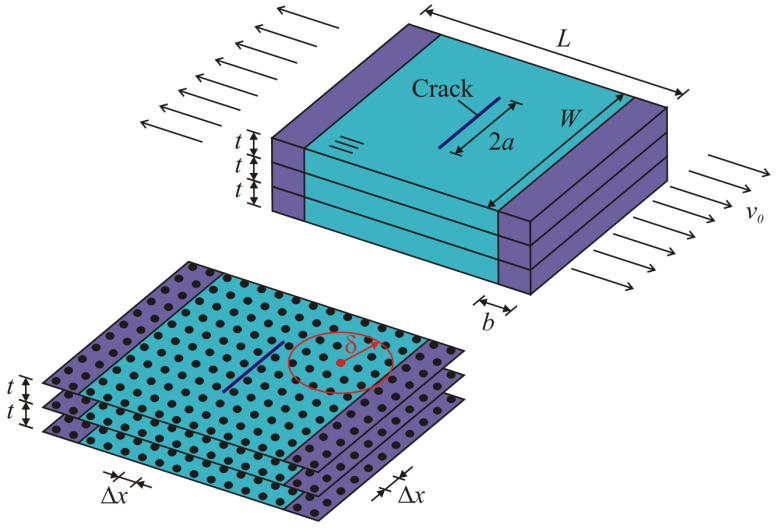

Figure 17. Loading and geometry of a composite laminate with a crack under tension loading.

analytically using (29) and (30) and are specified as $s_{in} = \varphi_c = 0.087$. The procedure for computing these critical stretch and angle values is explained in Appendix D.

For the [0°/90°/0°] laminate, an "H"-type splitting failure mode is observed for all plies, as shown in the left column of Figure 18. In this case, 0° plies are dominant in the loading direction; therefore, 0° plies determine the failure behavior of the laminate. However, in the [0°/45°/0°] laminate, a "Z"-type failure mode is obtained in all plies due to the presence of a 45° ply, as shown in Figure 18, right column. In both laminates, a delamination failure mode does not occur due to the high critical stretch values of interlayer and shear bonds with respect to fiber and matrix bonds.

If the bonding plies are weaker, smaller critical stretch and angle values can be specified for interlayer and shear bonds, respectively. If these parameters are specified as equal to the critical stretch of the matrix bond, that is, $s_{in} = \varphi_c = 0.0135$, the same intralayer failure modes are observed as in the previous case Figure 19. Also observed is the delamination failure mode between the plies due to the breakage of shear bonds around crack tip regions, shown in Figure 20. These damage patterns are consistent with those observed in [Bogert et al. 2006]. Consistent with their experimental observations, the effect of 45° ply has essentially a limited effect in the extent of the delamination except to influence the splitting mode of failure in the 0° layers.

6. Conclusions

Based on the numerical results, the peridynamic (PD) approach successfully predicts the damage growth patterns in fiber-reinforced laminates with preexisting cracks while considering the distinct properties of the fiber and matrix, as well as of the interlayer material between the plies. The predictions capture the correct failure mechanisms of matrix cracking, fiber breakage, and delamination without resorting to any special treatments, and agree with the experimental observations published in the literature. The simulations also capture failure modes among each ply, which are usually distinct; they heavily depend on fiber direction, which is realistically exhibited in the current results. It can be concluded that PD theory is a powerful method that can be employed for failure analysis of composite materials.

Appendix A: PD material constants of a lamina

As shown in Figures A.1 and A.2, a lamina is discretized with a single layer of material points in the thickness direction. The domain of integral H in (2) becomes a disk with radius δ and thickness t. The displacements of material points i and p are represented by $\boldsymbol{u}^{(i)}$ and $\boldsymbol{u}^{(p)}$, respectively. The initial relative position vector between these material points is denoted by

$$\boldsymbol{\xi} = \boldsymbol{x}^{(p)} - \boldsymbol{x}^{(i)}$$

and the relative displacement vector is

$$\boldsymbol{\eta} = \boldsymbol{u}^{(p)} - \boldsymbol{u}^{(i)}.$$

Similar to the determination of a PD material constant for an isotropic material [Oterkus et al. 2010], equating the strain energy density of a material point in a lamina computed using the PD theory and classical continuum mechanics results in the relationships between PD material constants, c_f and c_m, and engineering constants, E_1, E_2, G_{12}, and ν_{12}, as well as the coefficient of thermal expansion of a

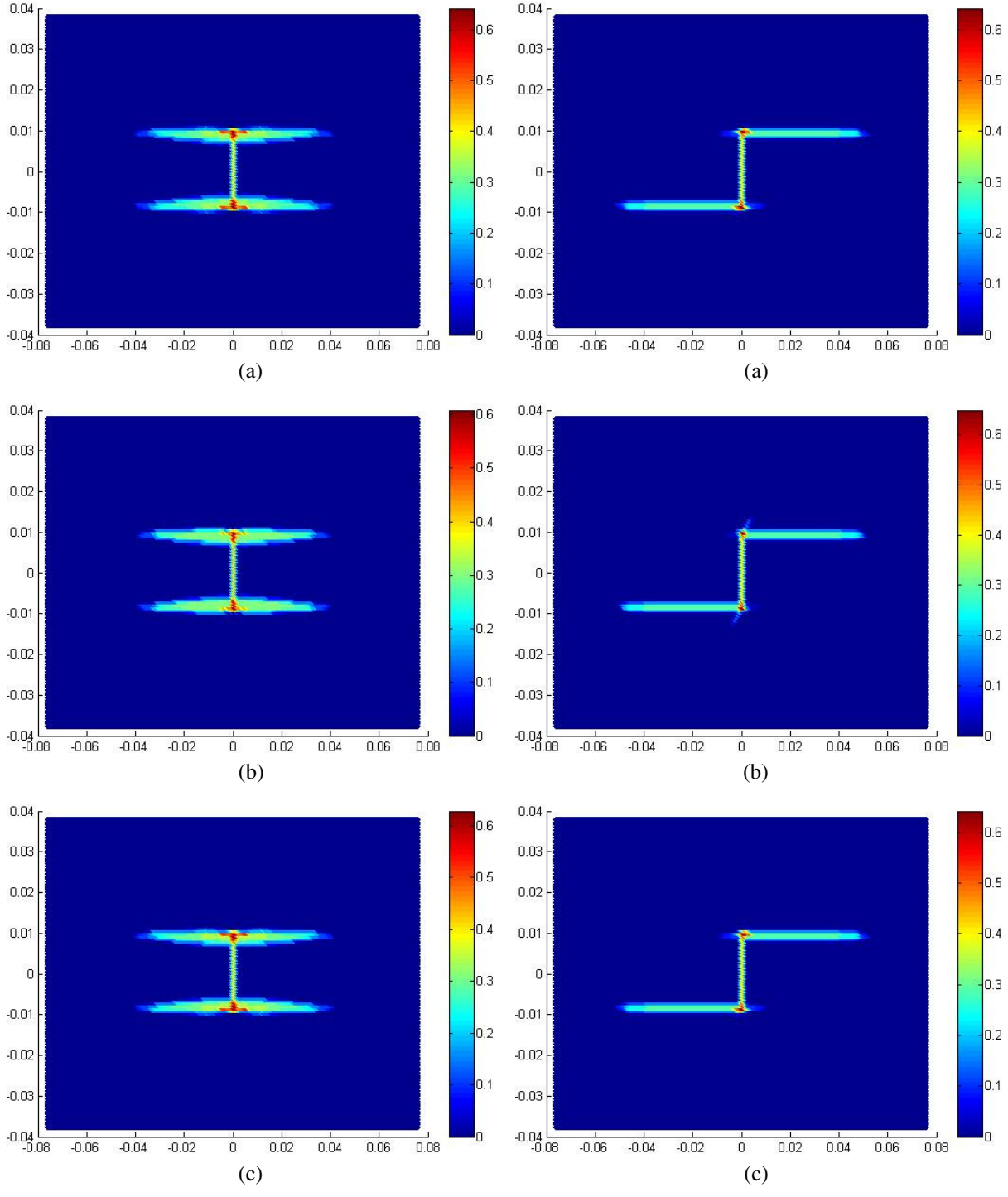

Figure 18. Matrix bond damage plots for a [0°/90°/0°] laminate (left column) and a [0°/45°/0°] laminate (right column) with a preexisting crack for $s_{\text{mt}} \neq s_{in} = \varphi_c$: (a) bottom ply, 0°; (b) center ply, 90° or 45°, and (c) top ply, 0°.

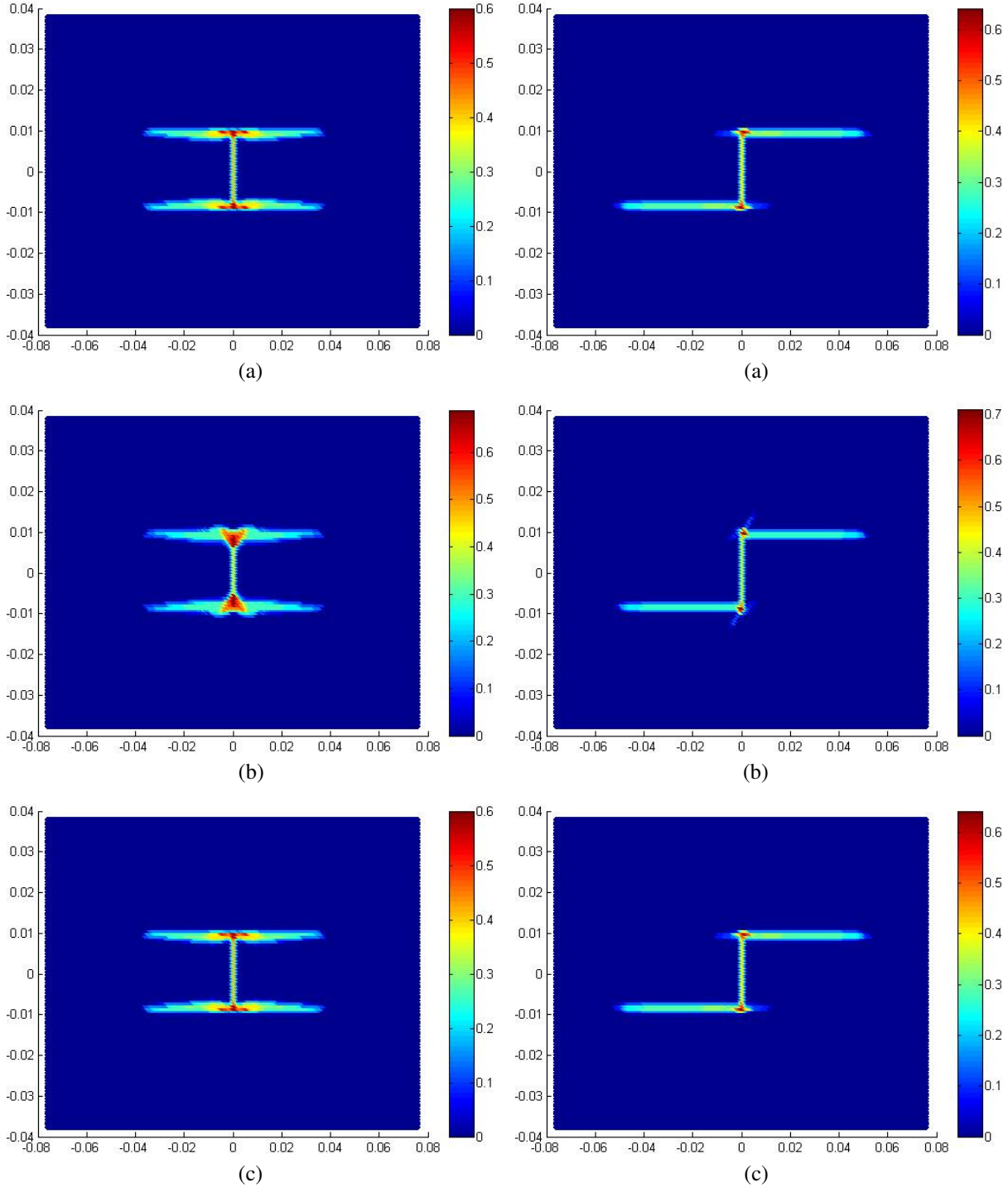

Figure 19. Matrix bond damage plots for a [0°/90°/0°] laminate (left column) and a [0°/45°/0°] laminate (right column) with a preexisting crack for $s_{\mathrm{mt}} = s_{i\mathrm{n}} = \varphi_c$: (a) bottom ply, 0°; (b) center ply, 90° or 45°, and (c) top ply, 0°.

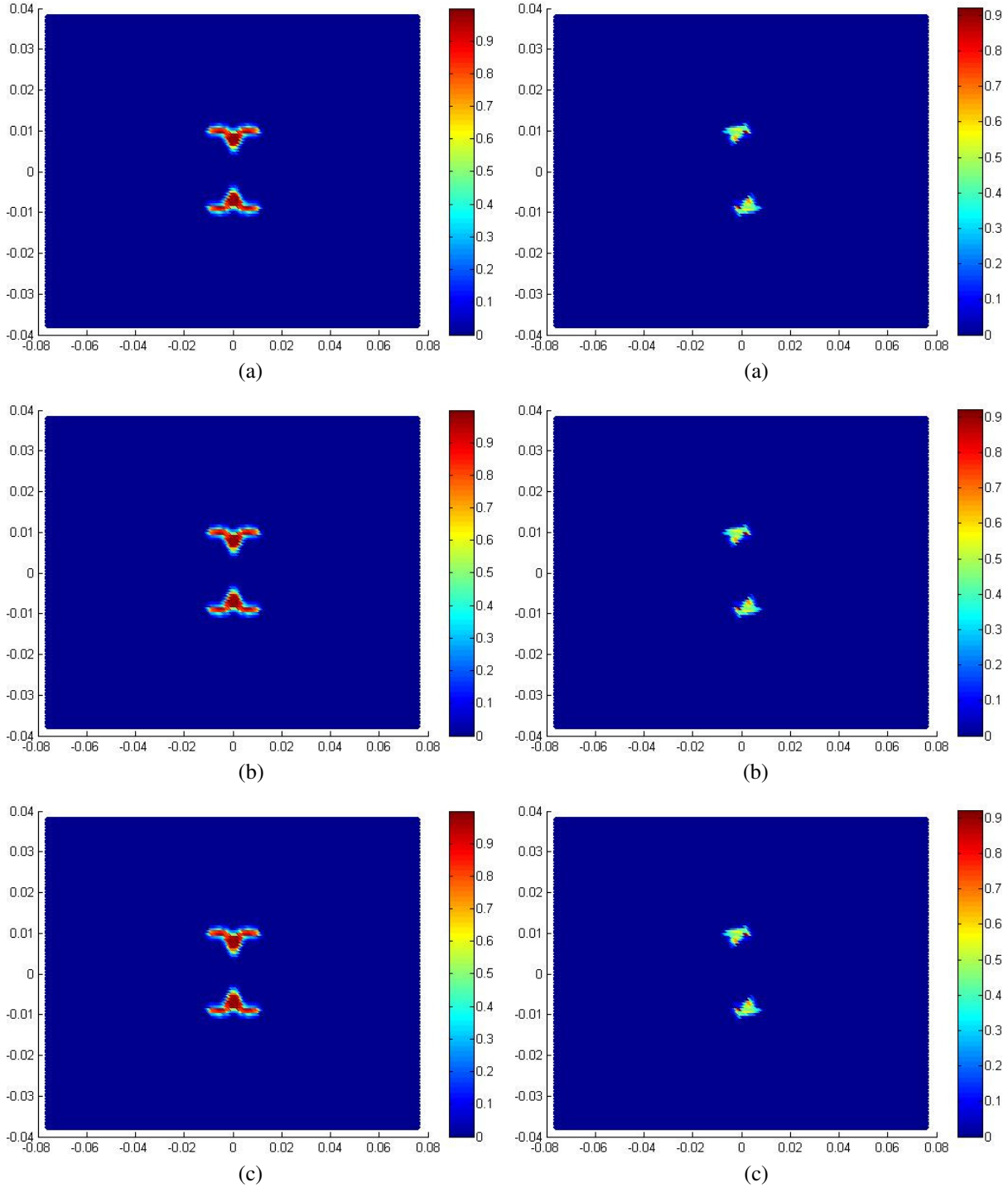

Figure 20. Shear bond damage plots for a [0°/90°/0°] laminate (left column) and a [0°/45°/0°] laminate (right column) with a preexisting crack for $s_{\mathrm{mt}} = s_{i\mathrm{n}} = \varphi_c$: (a) bottom ply, 0°; (b) center ply, 90° or 45°, and (c) top ply, 0°.

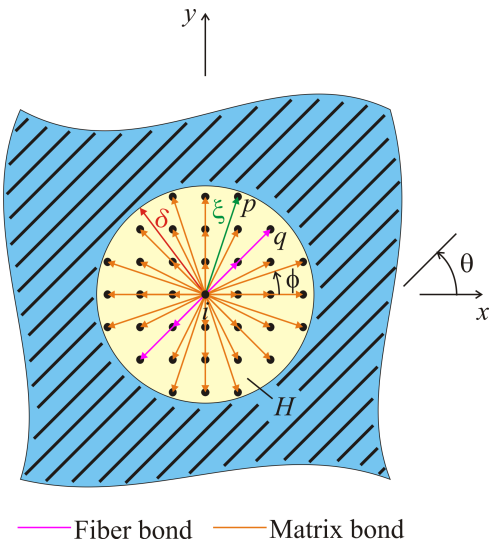

Figure A.1. PD horizon for a lamina with a fiber orientation of θ and PD bonds between material point i and other material points within its horizon.

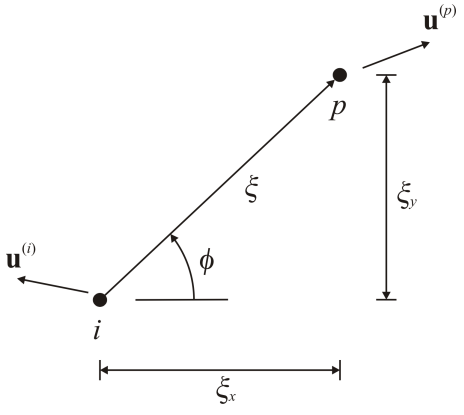

Figure A.2. PD bond between material points i and p with an orientation of ϕ.

PD bond, $\alpha(\phi)$, in terms of thermal expansion coefficients, α_x, α_y, and α_{xy}, for a lamina with a fiber orientation angle of θ.

The strain energy densities are calculated by considering a combined mechanical and thermal loading condition that results in a deformation, as shown in Figure A.3.

The strain field arising from such deformation can be expressed as

$$\epsilon_{xx} = \zeta, \qquad \epsilon_{yy} = -\nu_{xy}\zeta, \qquad \gamma_{xy} = -\mu_{xy}\zeta, \tag{A.1a}$$

where μ_{xy} is a parameter defined as

$$\mu_{xy} = \frac{m_x E_x}{E_1}, \tag{A.1b}$$

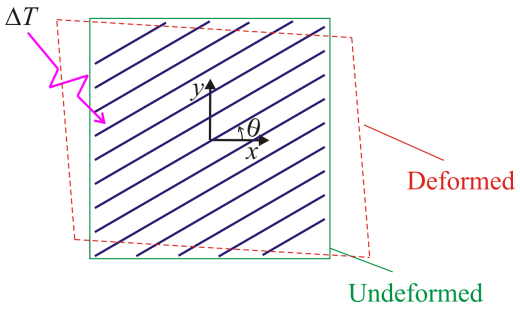

Figure A.3. Deformed configuration of an angle lamina subjected to a combined mechanical and thermal loading.

in which m_x is a nondimensional shear coupling term that relates the normal stress in the x-direction to the shear strain in the $(x$-$y)$ plane. This strain field represents the uniaxial tension loading in the absence of uniform temperature change, that is, $\Delta T = 0$. The contribution to the strain field from the uniform temperature change can be expressed as

$$\epsilon^*_{xx} = \alpha_x \Delta T, \qquad \epsilon^*_{yy} = \alpha_y \Delta T, \qquad \gamma^*_{xy} = \alpha_{xy} \Delta T. \tag{A.2}$$

Therefore, the contribution to the strain field from the mechanical loading becomes

$$\bar{\epsilon}_{xx} = \zeta - \alpha_x \Delta T, \qquad \bar{\epsilon}_{yy} = -\nu_{xy}\zeta - \alpha_y \Delta T, \qquad \bar{\gamma}_{xy} = -\mu_{xy}\zeta - \alpha_{xy} \Delta T. \tag{A.3}$$

Similarly, the stretch of a PD bond due to mechanical loading between material points i and p, $\bar{s}$, is the difference between the total stretch s and thermal stretch s^* as

$$\bar{s} = s - s^*. \tag{A.4}$$

The mechanical stretch, $\bar{s}$, can be expressed in terms of the relative displacement of the material points i and p, arising from the mechanical loading, along the X-direction (the direction of their initial relative position vector, $\boldsymbol{\xi}$) as

$$\bar{s} = \frac{\bar{u}^{(p)}_X - \bar{u}^{(i)}_X}{\xi}. \tag{A.5}$$

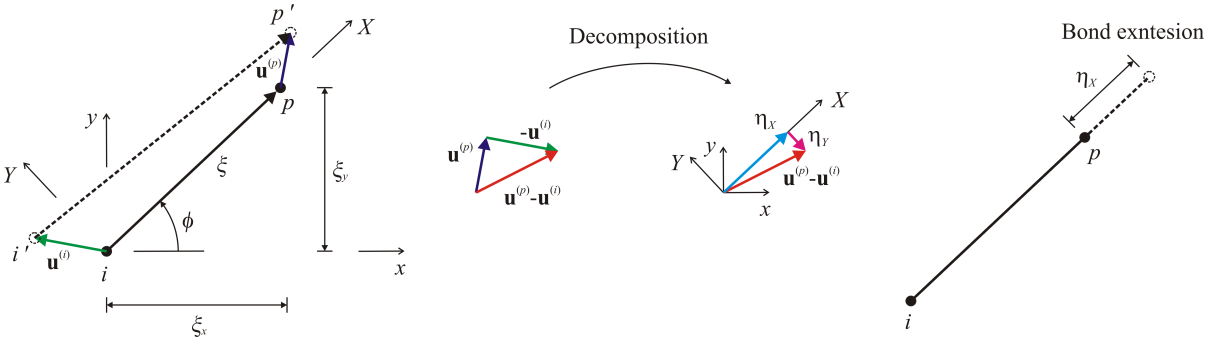

Figure A.4. Relative displacement between material points i and p.

As shown in Figure A.4, the relative displacement, $(\bar{u}_X^{(p)} - \bar{u}_X^{(i)})$, can be obtained in terms of the components of the displacement vectors $\bar{\boldsymbol{u}}^{(i)^T} = \{\bar{u}_x^{(i)}, \bar{u}_y^{(i)}\}^T$ and $\bar{\boldsymbol{u}}^{(p)^T} = \{\bar{u}_x^{(p)}, \bar{u}_y^{(p)}\}^T$ of the material points i and p, respectively. Coordinate transformation from an (x, y) coordinate system to an (X, Y) coordinate system leads to their explicit expressions as

$$\begin{Bmatrix} \bar{u}_X^{(p)} - \bar{u}_X^{(i)} \\ \bar{u}_Y^{(p)} - \bar{u}_Y^{(i)} \end{Bmatrix} = \begin{bmatrix} \cos(\phi) & \sin(\phi) \\ -\sin(\phi) & \cos(\phi) \end{bmatrix} \begin{Bmatrix} \bar{u}_x^{(p)} - \bar{u}_x^{(i)} \\ \bar{u}_y^{(p)} - \bar{u}_y^{(i)} \end{Bmatrix}. \tag{A.6}$$

Based on Figure A.5, the relative displacements of the material points i and p in the horizontal and vertical directions, $(\bar{u}_x^{(p)} - \bar{u}_x^{(i)})$ and $(\bar{u}_y^{(p)} - \bar{u}_y^{(i)})$, respectively, can also be obtained from

$$\bar{u}_x^{(p)} - \bar{u}_x^{(i)} = \bar{\epsilon}_{xx}\xi_x + \frac{\bar{\gamma}_{xy}}{2}\xi_y \tag{A.7a}$$

$$\bar{u}_y^{(p)} - \bar{u}_y^{(i)} = \frac{\bar{\gamma}_{xy}}{2}\xi_x + \bar{\epsilon}_{yy}\xi_y, \tag{A.7b}$$

where $\xi_x = \xi\cos(\phi)$ and $\xi_y = \xi\sin(\phi)$ are the components of the initial relative position vector, $\boldsymbol{\xi}$.

After invoking the mechanical strain components from (A.3) into (A.7a) and (A.7b) results in

$$\bar{u}_x^{(p)} - \bar{u}_x^{(i)} = \zeta\xi\left(\cos\phi - \frac{\mu_{xy}}{2}\sin\phi\right) - \xi\Delta T\left(\alpha_x\cos\phi + \frac{\alpha_{xy}}{2}\sin\phi\right), \tag{A.8a}$$

$$\bar{u}_y^{(p)} - \bar{u}_y^{(i)} = -\zeta\xi\left(\nu_{xy}\sin\phi + \frac{\mu_{xy}}{2}\cos\phi\right) - \xi\Delta T\left(\alpha_y\sin\phi + \frac{\alpha_{xy}}{2}\cos\phi\right). \tag{A.8b}$$

Using the coordinate transformation given in (A.6) along with (A.8), the mechanical stretch, $\bar{s}$, can be obtained in the form

$$\bar{s} = \zeta\left(\cos^2\phi - \mu_{xy}\sin\phi\cos\phi - \nu_{xy}\sin^2\phi\right) - \left(\alpha_x\cos^2\phi + \alpha_y\sin^2\phi + \alpha_{xy}\sin\phi\cos\phi\right)\Delta T. \tag{A.9}$$

Comparing this expression with (A.4) reveals that the expression in parentheses corresponds to the thermal expansion coefficient of the PD bond, $\alpha\phi$, defined as

$$\alpha\phi = \alpha_x\cos^2\phi + \alpha_y\sin^2\phi + \alpha_{xy}\sin\phi\cos\phi. \tag{A.10}$$

In the absence of thermal loading, that is, $\Delta T = 0^\circ$ in (A.9), the mechanical stretch reduces to

$$\bar{s} = s = \zeta\left(\cos^2\phi - \mu_{xy}\sin\phi\cos\phi - \nu_{xy}\sin^2\phi\right), \tag{A.11}$$

which represents the total stretch due to uniaxial tension. By using (7) in conjunction with (19), the strain energy density based on PD theory at a material point in a composite lamina can be evaluated as

$$\begin{aligned} U_{\mathrm{PD}} = {} & \frac{1}{2}\left(\frac{1}{2}\int_H c(\phi)\cos^4(\phi)\xi(\phi)\,dH - 2\nu_{xy}\int_H c(\phi)\sin^2(\phi)\cos^2(\phi)\xi(\phi)\,dH\right)\zeta^2 \\ & + \frac{1}{2}\left(-2\mu_{xy}\int_H c(\phi)\sin(\phi)\cos^3(\phi)\xi(\phi)\,dH + 2\nu_{xy}\mu_{xy}\int_H c(\phi)\sin^3(\phi)\cos(\phi)\xi(\phi)\,dH\right)\zeta^2 \\ & + \frac{1}{2}\left(\nu_{xy}^2\int_H c(\phi)\sin^4(\phi)\xi(\phi)\,dH + \mu_{xy}^2\int_H c(\phi)\sin^2(\phi)\cos^2(\phi)\xi(\phi)\,dH\right)\zeta^2. \end{aligned} \tag{A.12}$$

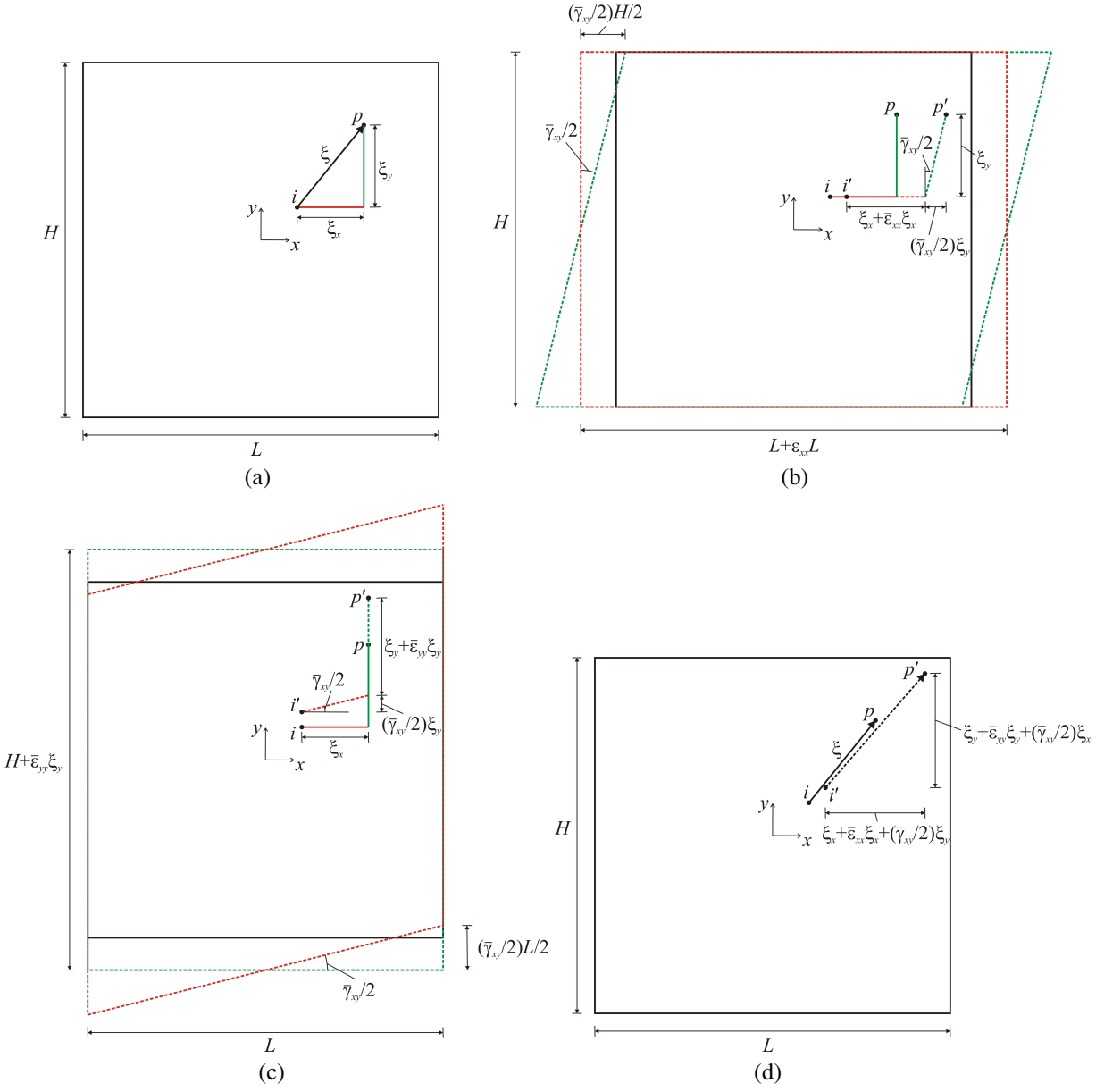

Figure A.5. Relative positions of points i and p: (a) undeformed state, (b) extension and simple shear in the x-direction, (c) extension and simple shear in the y-direction, and (d) extensions in x- and y-directions and pure shear.

Using (14) in conjunction with (16), the strain energy density of a material point based on classical continuum mechanics can be written as

$$U_E = \tfrac{1}{2}(\overline{Q}_{11} - 2\nu_{xy}\overline{Q}_{12} - 2\mu_{xy}\overline{Q}_{16} + 2\nu_{xy}\mu_{xy}\overline{Q}_{26} + \nu_{xy}^2\overline{Q}_{22} + \mu_{xy}^2\overline{Q}_{66})\zeta^2, \tag{A.13}$$

in which

$$\overline{Q}_{11} = Q_{11}\cos^4(\theta) + Q_{22}\sin^4(\theta) + 2(Q_{12} + 2Q_{66})\sin^2(\theta)\cos^2(\theta), \tag{A.14a}$$

$$\overline{Q}_{12} = (Q_{11} + Q_{22} - 4Q_{66})\sin^2(\theta)\cos^2(\theta) + Q_{12}\big(\cos^4(\theta) + \sin^4(\theta)\big), \tag{A.14b}$$

$$\overline{Q}_{16} = (Q_{11} - Q_{12} - 2Q_{66})\cos^3(\theta)\sin(\theta) - (Q_{22} - Q_{12} - 2Q_{66})\sin^3(\theta)\cos(\theta), \tag{A.14c}$$

$$\overline{Q}_{22} = Q_{11}\sin^4(\theta) + Q_{22}\cos^4(\theta) + 2(Q_{12} + 2Q_{66})\sin^2(\theta)\cos^2(\theta), \tag{A.14d}$$

$$\overline{Q}_{26} = (Q_{11} - Q_{12} - 2Q_{66})\cos(\theta)\sin^3(\theta) - (Q_{22} - Q_{12} - 2Q_{66})\cos^3(\theta)\sin(\theta), \tag{A.14e}$$

$$\overline{Q}_{66} = (Q_{11} + Q_{22} - 2Q_{12} - 2Q_{66})\sin^2(\theta)\cos^2(\theta) + Q_{66}\big(\sin^4(\theta) + \cos^4(\theta)\big), \tag{A.14f}$$

with

$$Q_{11} = \frac{E_1}{1 - \nu_{21}\nu_{12}}, \qquad Q_{12} = \frac{\nu_{12}E_2}{1 - \nu_{21}\nu_{12}}, \qquad Q_{22} = \frac{E_2}{1 - \nu_{21}\nu_{12}}, \qquad Q_{66} = G_{12}, \tag{A.15a}$$

provided that

$$1 - \nu_{12}\nu_{21} > 0 \tag{A.15b}$$

and subject to

$$\frac{\nu_{12}}{E_1} = \frac{\nu_{21}}{E_2}. \tag{A.15c}$$

Equating the coefficients of like terms in the strain energy density expressions from classical continuum theory, (A.13) and PD theory, (A.12), leads to

$$\overline{Q}_{11} = \frac{1}{2}\int_H c(\phi)\cos^4(\phi)\xi(\phi)\,dH, \tag{A.16a}$$

$$\overline{Q}_{12} = \frac{1}{2}\int_H c(\phi)\sin^2(\phi)\cos^2(\phi)\xi(\phi)\,dH, \tag{A.16b}$$

$$\overline{Q}_{16} = \frac{1}{2}\int_H c(\phi)\sin(\phi)\cos^3(\phi)\xi(\phi)\,dH, \tag{A.16c}$$

$$\overline{Q}_{22} = \frac{1}{2}\int_H c(\phi)\sin^4(\phi)\xi(\phi)\,dH, \tag{A.16d}$$

$$\overline{Q}_{26} = \frac{1}{2}\int_H c(\phi)\sin^3(\phi)\cos(\phi)\xi(\phi)\,dH, \tag{A.16e}$$

$$\overline{Q}_{66} = \frac{1}{2}\int_H c(\phi)\sin^2(\phi)\cos^2(\phi)\xi(\phi)\,dH. \tag{A.16f}$$

Using the approximation given in (20), (A.16) can be rewritten in the form

$$\overline{Q}_{11} = \frac{1}{2}\sum_{q=1}^{Q} c_f \cos^4(\theta)\xi_{qi} V_q + \frac{t}{2}\int_0^{2\pi}\int_0^{\delta} c_m\big(\cos^4(\phi)\xi\big)\xi\, d\xi d\phi, \tag{A.17a}$$

$$\overline{Q}_{12} = \frac{1}{2}\sum_{q=1}^{Q} c_f \sin^2(\theta)\cos^2(\theta)\xi_{qi} V_q + \frac{t}{2}\int_0^{2\pi}\int_0^{\delta} c_m\big(\sin^2(\phi)\cos^2(\phi)\xi\big)\xi\, d\xi d\phi, \tag{A.17b}$$

$$\overline{Q}_{16} = \frac{1}{2}\sum_{q=1}^{Q} c_f \sin(\theta)\cos^3(\theta)\xi_{qi} V_q + \frac{t}{2}\int_0^{2\pi}\int_0^{\delta} c_m\big(\sin(\phi)\cos^3(\phi)\xi\big)\xi\, d\xi d\phi, \tag{A.17c}$$

$$\overline{Q}_{22} = \frac{1}{2}\sum_{q=1}^{Q} c_f \sin^4(\theta)\xi_{qi} V_q + \frac{t}{2}\int_0^{2\pi}\int_0^{\delta} c_m\big(\sin^4(\phi)\xi\big)\xi\, d\xi d\phi, \tag{A.17d}$$

$$\overline{Q}_{26} = \frac{1}{2}\sum_{q=1}^{Q} c_f \sin^3(\theta)\cos(\theta)\xi_{qi} V_q + \frac{t}{2}\int_0^{2\pi}\int_0^{\delta} c_m\big(\sin^3(\phi)\cos(\phi)\xi\big)\xi\, d\xi d\phi, \tag{A.17e}$$

$$\overline{Q}_{66} = \frac{1}{2}\sum_{q=1}^{Q} c_f \sin^2(\theta)\cos^2(\theta)\xi_{qi} V_q + \frac{t}{2}\int_0^{2\pi}\int_0^{\delta} c_m\big(\sin^2(\phi)\cos^2(\phi)\xi\big)\xi\, d\xi d\phi. \tag{A.17f}$$

Performing the integrations in (A.17) results in the relations between the engineering constants and the PD material constants, c_f and c_m, as

$$\overline{Q}_{11} = \big(\beta\cos^4(\theta)\big)c_f + \frac{\pi t\delta^3}{8}c_m, \tag{A.18a}$$

$$\overline{Q}_{12} = \big(\beta\sin^2(\theta)\cos^2(\theta)\big)c_f + \frac{\pi t\delta^3}{24}c_m, \tag{A.18b}$$

$$\overline{Q}_{16} = \big(\beta\sin(\theta)\cos^3(\theta)\big)c_f, \tag{A.18c}$$

$$\overline{Q}_{22} = \big(\beta\sin^4(\theta)\big)c_f + \frac{\pi t\delta^3}{8}c_m, \tag{A.18d}$$

$$\overline{Q}_{26} = \big(\beta\sin^3(\theta)\cos(\theta)\big)c_f, \tag{A.18e}$$

$$\overline{Q}_{66} = \big(\beta\sin^2(\theta)\cos^2(\theta)\big)c_f + \frac{\pi t\delta^3}{24}c_m, \tag{A.18f}$$

where

$$\beta = \frac{1}{2}\sum_{q=1}^{Q}\xi_{qi} V_q. \tag{A.19}$$

Examination of these equations show that the right-hand sides of (A.18b) and (A.18f) are the same, requiring that

$$\overline{Q}_{12} = \overline{Q}_{66}. \tag{A.20}$$

Substituting from (A.14b) and (A.14f) into (A.20) leads to

$$Q_{12} = Q_{66}. \tag{A.21}$$

Examination of (A.18c) and (A.18e) reveals that

$$\beta c_f = \frac{\overline{Q}_{16}}{\sin(\theta)\cos^3(\theta)} = \frac{\overline{Q}_{26}}{\sin^3(\theta)\cos(\theta)}. \tag{A.22}$$

Invoking the requirement given by (A.21) into (A.14c) and (A.14e) renders this equation as

$$(Q_{11} - 3Q_{12}) - (Q_{22} - 3Q_{12})\frac{\sin^2(\theta)}{\cos^2(\theta)} = (Q_{11} - 3Q_{12}) - (Q_{22} - 3Q_{12})\frac{\cos^2(\theta)}{\sin^2(\theta)}. \tag{A.23}$$

For this equation to be valid for all fiber orientation, it is required that

$$Q_{22} = 3Q_{12}. \tag{A.24}$$

After invoking the requirements given by (A.21) and (A.24) into (A.14a) and (A.14d), subtracting (A.18d) from (A.18a) results in

$$c_f = \frac{Q_{11} - Q_{22}}{\beta}. \tag{A.25}$$

Similarly, invoking the requirements given by (A.21) and (A.24) into (A.14a) and substituting from (A.25) into (A.18a) leads to

$$c_m = \frac{24Q_{12}}{\pi t \delta^3}. \tag{A.26}$$

The expressions for the bond constants, c_f and c_m, given by (A.25) and (A.26), as well as the relations given (A.21) and (A.24), can be rewritten in terms of the engineering constants as

$$c_f = \frac{2E_1(E_1 - E_2)}{(E_1 - \frac{1}{9}E_2)\left(\sum_{q=1}^{Q} \xi_{qi} V_q\right)}, \quad c_m = \frac{8E_1E_2}{(E_1 - \frac{1}{9}E_2)\pi t \delta^3}, \quad G_{12} = \frac{\nu_{12}E_2}{1 - \nu_{21}\nu_{12}}, \quad \nu_{12} = \frac{1}{3}. \tag{A.27}$$

Appendix B: Surface correction factors for a composite lamina

The surface correction factors for fiber and matrix bonds are determined by computing the strain energy density at two distinct material points under uniaxial strain conditions in the x-, and y-directions, that is, $\epsilon_{xx} \neq 0$, $\epsilon_{yy} = \gamma_{xy} = 0$ and $\epsilon_{yy} \neq 0$, $\epsilon_{xx} = \gamma_{xy} = 0$. The first material point located near an external surface has a truncated horizon, as shown in Figure B.1. The second material point is located far away from an external boundary and is completely embedded in a single lamina, as shown in Figure B.2.

The strain energy density of a material point at $\boldsymbol{x}$ is decomposed as

$$W = W_{(f)} + W_{(m)}, \tag{B.1}$$

where $W_{(f)}(x)$ and $W_{(m)}(x)$ represent the contribution of fiber bonds and matrix bonds, respectively.

First, uniaxial strain loading is applied in the x-direction, and the resulting displacement field can be expressed at material point $\boldsymbol{x}$ as

$$\boldsymbol{u}^T(\boldsymbol{x}) = \left\{ \frac{\partial u_x^*}{\partial x} x \;\; 0 \right\}, \tag{B.2}$$

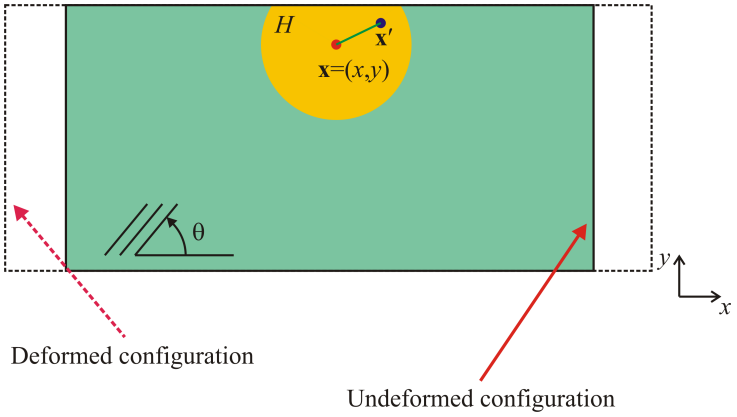

Figure B.1. Material point $\boldsymbol{x}$ with a truncated horizon in a lamina.

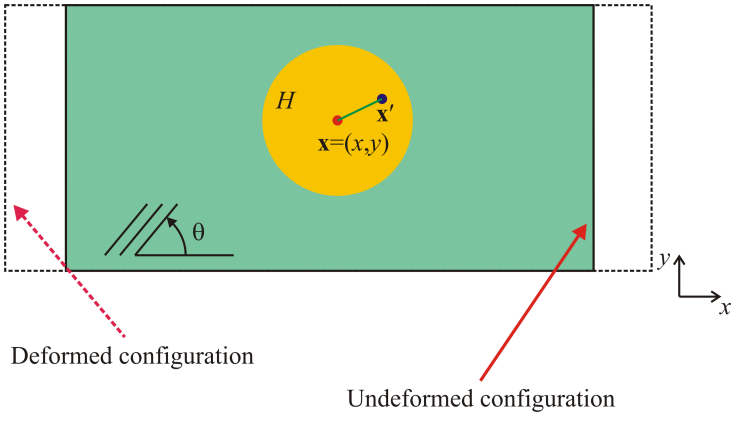

Figure B.2. Material point $\boldsymbol{x}$ far away from external surfaces of a lamina.

in which $\partial u_x^*/\partial x$ is the applied constant displacement gradient. The strain energy density, $W_x(\boldsymbol{x})$, due to this applied displacement gradient is expressed as

$$W_x(\boldsymbol{x}) = \int_H w(\boldsymbol{u}' - \boldsymbol{u}, \boldsymbol{x}' - \boldsymbol{x})\, dH, \tag{B.3}$$

where H represents the horizon of the material point at $\boldsymbol{x}$ and w represents the strain energy density of the PD bond between material points at $\boldsymbol{x}$ and $\boldsymbol{x}'$. The strain energy density, $W_y(\boldsymbol{x})$, of the material point at $\boldsymbol{x}$ can also be computed due to uniaxial strain in the y-direction. The subscripts $x$and y denote uniaxial strain loading condition in x- and y-directions, respectively.

In accordance with (B.1), the strain energy density at material point $\boldsymbol{x}$ due to the applied uniaxial strain loading in x- and y-directions can be decomposed as

$$W_x = W_{(f)x} + W_{(m)x}, \qquad W_y = W_{(f)y} + W_{(m)y}. \tag{B.4}$$

With this decomposition, the strain energy density vectors, $\boldsymbol{W}_{(f)}(\boldsymbol{x})$ and $\boldsymbol{W}_{(m)}(\boldsymbol{x})$, can be formed as

$$\boldsymbol{W}_{(f)}^{T}(\boldsymbol{x}) = \left\{ W_{(f)x} \;\; W_{(f)y} \right\}, \qquad \boldsymbol{W}_{(m)}^{T}(\boldsymbol{x}) = \left\{ W_{(m)x} \;\; W_{(m)y} \right\}, \tag{B.5}$$

where $\boldsymbol{W}_{(f)}(\boldsymbol{x})$ and $\boldsymbol{W}_{(m)}(\boldsymbol{x})$ represent the contribution of fiber bonds and matrix bonds to the strain energy density of the material point at $\boldsymbol{x}$, respectively.

For both fiber and matrix bonds, the correction factors corresponding to the two loading directions can be defined as the ratio of the strain energy density of the material point embedded far away from an external surface in a lamina, $W_{(\beta)\alpha}^{(\infty)}$, to that of a material point near an external surface with a truncated horizon, $W_{(\beta)\alpha}$, with $\alpha = x, y$ and $\beta = f, m$. For a material point whose horizon is completely embedded in a single lamina, the strain energy densities for the uniaxial strain loading condition in the x- and y-directions can be computed using classical continuum mechanics as

$$W_{x}^{(\infty)} = \tfrac{1}{2}\,\overline{Q}_{11}\zeta^{2}, \qquad W_{y}^{(\infty)} = \tfrac{1}{2}\,\overline{Q}_{22}\zeta^{2}, \tag{B.6}$$

where $\overline{Q}_{11}$ and $\overline{Q}_{22}$ are the coefficients of the transformed reduced stiffness matrix $\overline{\boldsymbol{Q}}$ [Kaw 2006]. The strain energy densities given by (B.6) can be decomposed into two parts which are associated with the deformations of fiber and matrix materials, that is, $W_{(\beta)\alpha}^{(\infty)}$, with $\alpha = x, y$ and $\beta = f, m$, as

$$W_{x}^{(\infty)} = W_{(f)x}^{(\infty)} + W_{(m)x}^{(\infty)}, \qquad W_{y}^{(\infty)} = W_{(f)y}^{(\infty)} + W_{(m)y}^{(\infty)}. \tag{B.7}$$

However, the explicit form of this decomposition is not known because each lamina is treated as homogeneous and orthotropic within the realm of classical continuum mechanics. Therefore, this decomposition is assumed similar in form to that of between c_f and c_m as given by (A.18a) and (A.18d), respectively. This assumption leads to the following decomposition of strain energies given by (B.6) in the form

$$W_{x}^{(\infty)} = \overline{W}_{(f)}^{(\infty)}\cos^{4}(\theta) + \overline{W}_{(m)}^{(\infty)} \qquad W_{y}^{(\infty)} = \overline{W}_{(f)}^{(\infty)}\sin^{4}(\theta) + \overline{W}_{(m)}^{(\infty)}, \tag{B.8}$$

where $\overline{W}_{(f)}^{(\infty)}$ and $\overline{W}_{(m)}^{(\infty)}$, representing the contribution of fiber and matrix materials, respectively, are to be determined. Substituting for the strain energy density expressions given by (B.8) in (B.6) permits the determination of $\overline{W}_{(f)}^{(\infty)}$ and $\overline{W}_{(m)}^{(\infty)}$ in terms of the material constants $\overline{Q}_{11}$ and $\overline{Q}_{22}$ as

$$\overline{W}_{(f)}^{(\infty)} = \frac{1}{2}\left\{ \frac{(\overline{Q}_{11} - \overline{Q}_{22})}{\cos^{4}(\theta) - \sin^{4}(\theta)} \right\}\zeta^{2}, \qquad \overline{W}_{(m)}^{(\infty)} = \frac{1}{2}\left\{ \frac{\left(\overline{Q}_{22}\cos^{4}(\theta) - \overline{Q}_{11}\sin^{4}(\theta)\right)}{\cos^{4}(\theta) - \sin^{4}(\theta)} \right\}\zeta^{2}. \tag{B.9}$$

The final form of the terms, $W_{(\beta)\alpha}^{(\infty)}$, with $\alpha = x, y$ and $\beta = f, m$, in (B.7) can be written as

$$W_{(f)x}^{(\infty)} = \frac{1}{2}\left\{ \frac{(\overline{Q}_{11} - \overline{Q}_{22})\cos^{4}(\theta)}{\cos^{4}(\theta) - \sin^{4}(\theta)} \right\}\zeta^{2}, \tag{B.10a}$$

$$W_{(m)x}^{(\infty)} = \frac{1}{2}\left\{ \frac{\left(\overline{Q}_{22}\cos^{4}(\theta) - \overline{Q}_{11}\sin^{4}(\theta)\right)}{\cos^{4}(\theta) - \sin^{4}(\theta)} \right\}\zeta^{2}, \tag{B.10b}$$

$$W_{(f)y}^{(\infty)} = \frac{1}{2}\left\{ \frac{(\overline{Q}_{11} - \overline{Q}_{22})\sin^{4}(\theta)}{\cos^{4}(\theta) - \sin^{4}(\theta)} \right\}\zeta^{2}, \tag{B.10c}$$

$$W_{(m)y}^{(\infty)} = \frac{1}{2}\left\{ \frac{\left(\overline{Q}_{22}\cos^{4}(\theta) - \overline{Q}_{11}\sin^{4}(\theta)\right)}{\cos^{4}(\theta) - \sin^{4}(\theta)} \right\}\zeta^{2}. \tag{B.10d}$$

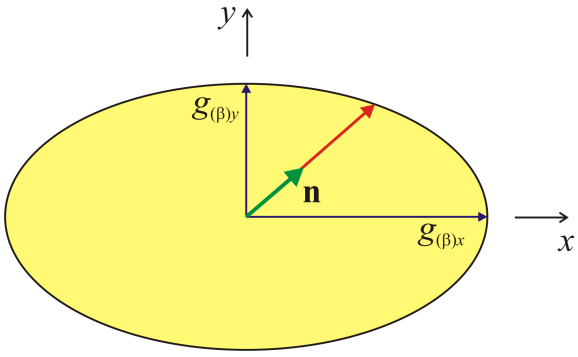

Figure B.3. Construction of an ellipse for surface correction factors.

With these values, a vector of correction factors for fiber and matrix bonds at material point $\boldsymbol{x}$ can be formed as

$$\boldsymbol{g}_{(\beta)}(\boldsymbol{x}) = \{g_{(\beta)x}, g_{(\beta)y}\}^T = \{W^{(\infty)}_{(\beta)x}/W_{(\beta)x}, W^{\infty}_{(\beta)y}/W_{(\beta)y}\}^T, \qquad \text{with } \beta = f, m. \tag{B.11}$$

These correction factors are only based on loading in the x- and y-directions. However, they can be used as the principal values of an ellipse in order to approximate the surface correction factor in an arbitrary direction of unit vector, $\boldsymbol{n}$ (Figure B.3).

In the case of a surface correction factor for a PD bond between material points $\boldsymbol{x}_{(i)}$ and $\boldsymbol{x}_{(j)}$ under general loading conditions, shown in Figure B.4a, the correction factors in the direction of the relative position vector, $\boldsymbol{n} = \boldsymbol{\xi}/|\boldsymbol{\xi}| = \{n_x, n_y\}^T$, in the undeformed configuration between these two material points, can be obtained in a similar manner.

A vector of correction factors at material points, $\boldsymbol{x}_{(i)}$ and $\boldsymbol{x}_{(j)}$ can be formed as

$$\boldsymbol{g}_{(\beta)(i)}(\boldsymbol{x}_{(i)}) = \{g_{(\beta)x(i)}, g_{(\beta)y(i)}\}^T = \{W^{(\infty)}_{(\beta)x}/W_{(\beta)x(i)}, W^{(\infty)}_{(\beta)y}/W_{(\beta)y(i)}\}^T, \tag{B.12}$$

$$\boldsymbol{g}_{(\beta)(j)}(\boldsymbol{x}_{(j)}) = \{g_{(\beta)x(j)}, g_{(\beta)y(j)}\}^T = \{W^{(\infty)}_{(\beta)x}/W_{(\beta)x(j)}, W^{(\infty)}_{(\beta)y}/W_{(\beta)y(j)}\}^T. \tag{B.13}$$

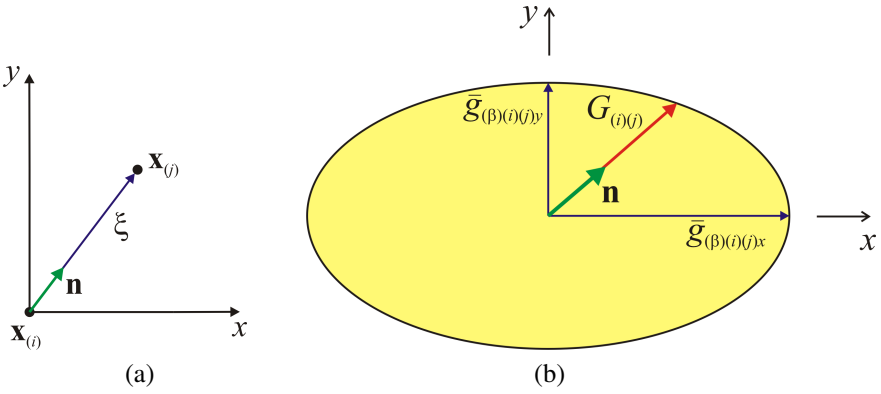

Figure B.4. (a) PD bond between material points at $x_{(i)}$ and $x_{(j)}$ (left) and (b) the ellipse for the surface correction factor.

These correction factors are, in general, different at material points $\boldsymbol{x}_{(i)}$ and $\boldsymbol{x}_{(j)}$. Therefore, the correction factor for a PD bond between material points $\boldsymbol{x}_{(i)}$ and $\boldsymbol{x}_{(j)}$ can be obtained by their mean values as

$$\bar{\boldsymbol{g}}_{(\beta)(i)(j)} = \{\bar{g}_{(\beta)(i)(j)x}, \bar{g}_{(\beta)(i)(j)y}\}^T = (\boldsymbol{g}_{(\beta)(i)} + \boldsymbol{g}_{(\beta)(j)})/2, \tag{B.14}$$

which can be used as the principal values of an ellipse, as shown in Figure B.4. The intersection of the ellipse and a relative position vector of material points $\boldsymbol{x}_{(i)}$ and $\boldsymbol{x}_{(j)}$, $\boldsymbol{n}$, provides the correction factors as

$$G_{(\beta)(i)(j)} = \left([n_x/\bar{g}_{(\beta)(i)(j)x}]^2 + [n_y/\bar{g}_{(\beta)(i)(j)y}]^2\right)^{-\frac{1}{2}}. \tag{B.15}$$

After considering the surface effects, the discrete form of the equations of motion given in (13) is corrected as

$$\rho(\boldsymbol{x}_{(i)})\ddot{\boldsymbol{u}}(\boldsymbol{x}_{(i)}, t) = \sum_{j=1}^{M} \begin{pmatrix} a_{(i)(j)} G_{(f)(i)(j)} \boldsymbol{f}\left(\boldsymbol{u}(\boldsymbol{x}_{(j)}, t) - \boldsymbol{u}(\boldsymbol{x}_{(i)}, t), \boldsymbol{x}_{(j)} - \boldsymbol{x}_{(i)}\right) + \\ b_{(i)(j)} G_{(m)(i)(j)} \boldsymbol{f}\left(\boldsymbol{u}(\boldsymbol{x}_{(j)}, t) - \boldsymbol{u}(\boldsymbol{x}_{(i)}, t), \boldsymbol{x}_{(j)} - \boldsymbol{x}_{(i)}\right) \end{pmatrix} V_{(j)} + \boldsymbol{b}(\boldsymbol{x}_{(i)}, t). \tag{B.16}$$

where the coefficients $a_{(i)(j)}$ and $b_{(i)(j)}$ take a value of either 1 or 0 if the interaction between material points $\boldsymbol{x}_{(i)}$ and $\boldsymbol{x}_{(j)}$ is a fiber bond or a matrix bond, respectively.

Based on numerical experimentation with varying values of displacement gradients, there is no significant effect on the surface corrections. Thus, the displacement gradient $\partial u_x^*/\partial x$ is assigned a value of 0.001.

Appendix C: PD interlayer and shear bond constants of a laminate

The interlayer bond constant, c_{in}, and the shear bond constant, c_{is}, shown in Figure C.1, can be expressed in terms of engineering constants based on the transverse normal and shear deformation response of the isotropic matrix material by equating the total strain energy density of interlayer and shear bonds

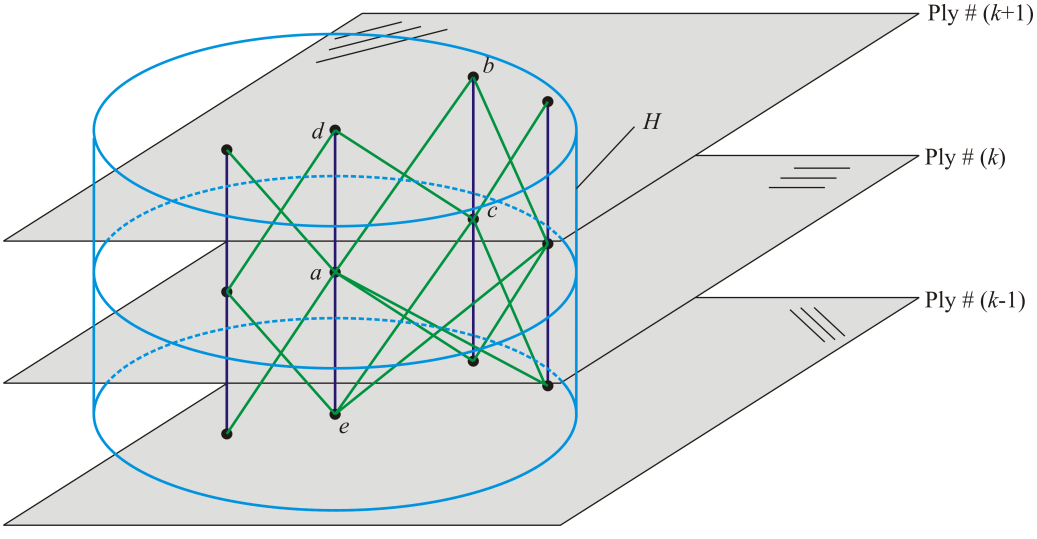

Figure C.1. Interlayer and shear bonds between neighboring plies (only some of the interactions are depicted explicitly for clarity).

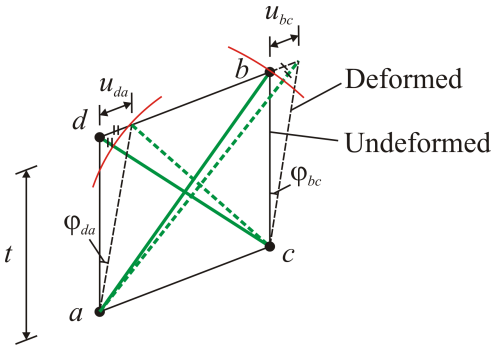

Figure C.2. Shear bonds between material points b and a, and between material points d and c, in both undeformed and deformed configurations.

calculated from PD theory and classical continuum mechanics. The strain energy density of the interlayer bonds associated with the material point a can be computed by summing the strain energy density of the two interlayer bonds between material points d and e and the material point a (Figure C.1). It can be readily obtained by multiplying the micropotential given in (8a) with the material volume.

Furthermore, the strain energy density of shear bonds can be obtained by using $(28)_2$ in conjunction with (7). Thus, the total strain energy density due to the interlayer and shear bonds can be computed as

$$U_{\mathrm{PD}} = \frac{1}{2}\sum_{j=d,e}\frac{c_{in}s_{ja}^2\xi_{ja}}{2}V_j + \frac{1}{2}\int_H \frac{c_{is}\varphi^2}{2}\,dH. \tag{C.1}$$

The expression for the shear angle in (C.1) is obtained by determining the average shear angle inside the quadrilateral formed by material points a, b, c, and d, as shown in Figure C.2. Averaging is achieved by computing the shear angles along the lines between material points a and d, and b and c, which are defined as φ_{da} and φ_{bc}, respectively.

These shear angles are obtained from the ratio of the displacements u_{da} and u_{bc} of material points d and b with respect to a and c, respectively, to the ply thickness, t, as

$$\varphi_{da} = \frac{u_{da}}{t}, \qquad \varphi_{bc} = \frac{u_{bc}}{t}. \tag{C.2}$$

The relative displacements u_{da} and u_{bc} are approximated as the change in length of the bonds between material points d and c, and b and a, respectively,

$$u_{da} = -\big(|\boldsymbol{\xi}_{dc} + \boldsymbol{\eta}_{dc}| - |\boldsymbol{\xi}_{dc}|\big), \tag{C.3a}$$

$$u_{bc} = |\boldsymbol{\xi}_{ba} + \boldsymbol{\eta}_{ba}| - |\boldsymbol{\xi}_{ba}|. \tag{C.3b}$$

Note that the minus sign in (C.3a) arises due to the contraction of the shear bond between material points d and c, whereas the bond between material points b and a extends. The average value of the shear strains φ_{da} and φ_{bc} results in

$$\varphi = \frac{\varphi_{da} + \varphi_{bc}}{2} = \frac{(|\boldsymbol{\xi}_{ba} + \boldsymbol{\eta}_{ba}| - |\boldsymbol{\xi}_{ba}|) - (|\boldsymbol{\xi}_{dc} + \boldsymbol{\eta}_{dc}| - |\boldsymbol{\xi}_{dc}|)}{2t}, \tag{C.4}$$

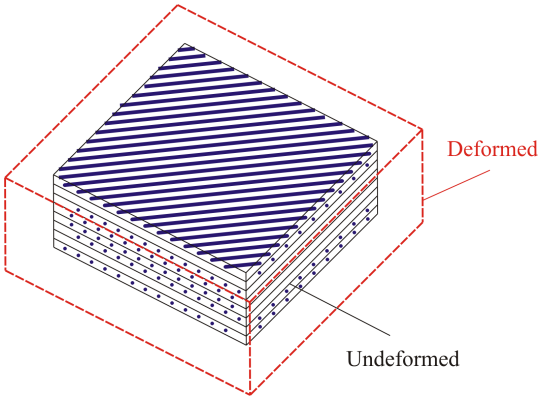

Figure C.3. A composite laminate subjected to isotropic expansion loading.

where $\boldsymbol{\xi}_{ba}$ and $\boldsymbol{\xi}_{dc}$ correspond to the bond vectors between material points b and a, and between material points d and c, respectively. Similarly, the vectors $\boldsymbol{\eta}_{ba}$ and $\boldsymbol{\eta}_{dc}$ are the relative displacement vectors between material points b and a, and between material points d and c, respectively.

In order to obtain the interlayer bond constant, the laminate is subjected to an isotropic expansion loading of $s = \zeta$, as shown in Figure C.3.

For a material point, a, located in the k-th ply of the laminate (Figure C.4), the contributions of the interlayer and shear bonds to the strain energy density of the material point due to isotropic expansion loading can be calculated using (C.1)

$$U_{\mathrm{PD}} = \frac{1}{2} \sum_{j=d,e} \frac{c_{in} s_{ja}^2 \xi_{ja}}{2} V_j. \tag{C.5}$$

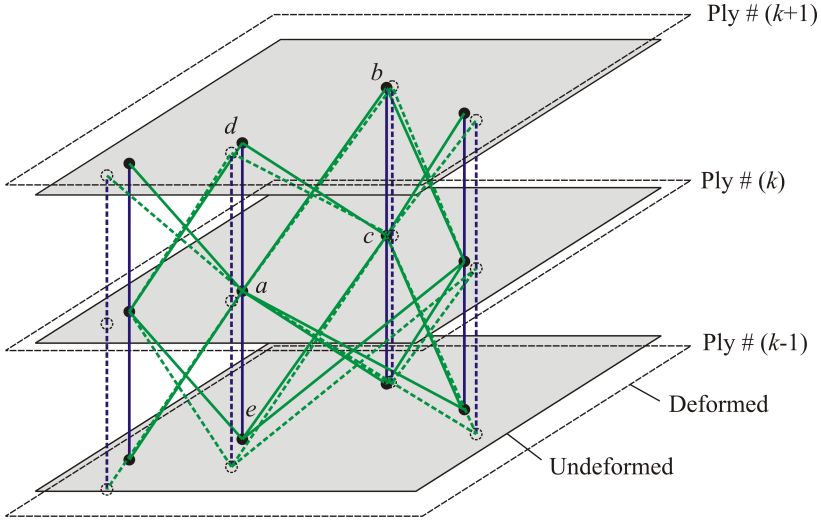

Figure C.4. Deformation of interlayer and shear bonds between neighboring plies (only some of the interactions are depicted explicitly for clarity).

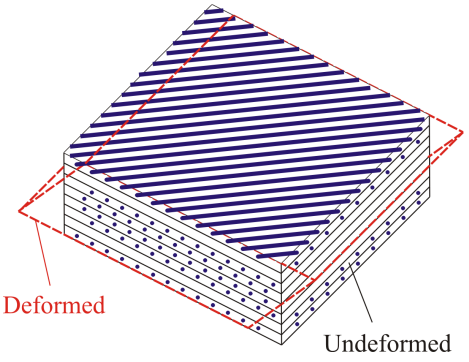

Figure C.5. A composite laminate subjected to simple shear loading.

Note that the shear strain, φ, defined in (C.2) has a zero value for this loading condition because the relative displacements u_{da} and u_{bc} given in (C.3a) and (C.3b) are equal in magnitude with opposite signs. Therefore, shear bonds do not have any contribution to the strain energy density for this loading condition. Both of the bond lengths ξ_{da} and ξ_{ea} are equivalent to the ply thickness, t. Therefore, for this loading condition, (C.5) can be evaluated as

$$U_{\mathrm{PD}} = \frac{c_{in}\zeta^2 t\overline{V}}{2}, \tag{C.6}$$

where $\overline{V}$ is equal to the volume of material points d and e, that is, $\overline{V} = V_d = V_e$.

The corresponding strain energy density of the material point for the same loading condition can be calculated using classical continuum mechanics as

$$U_E = \tfrac{1}{2} E_m \zeta^2, \tag{C.7}$$

with E_m representing the elastic modulus of the matrix material. Equating strain energy densities from (C.6) and (C.7) results in the relation between the interlayer bond constant, c_{in}, as

$$c_{in} = \frac{E_m}{t\overline{V}}. \tag{C.8}$$

The shear bond constant, c_{is}, can be evaluated similarly. In this case, the laminate is subjected to a simple shear loading of $\gamma = \zeta$, as shown in Figure C.5. For this loading condition, the interlayer bonds do not extend (Figure C.6). Therefore, their stretch values are zero. Hence, the interlayer bonds do not contribute to the strain energy density of the laminate.

As shown in Figure C.7, the original and deformed lengths of the shear bond between material points b and a can be expressed as

$$|\boldsymbol{\xi}_{ba}| = \sqrt{\ell^2 + t^2}, \tag{C.9a}$$

$$|\boldsymbol{\xi}_{ba} + \boldsymbol{\eta}_{ba}| = \sqrt{\bar{\ell}^2 + t^2}, \tag{C.9b}$$

where t is the ply thickness.

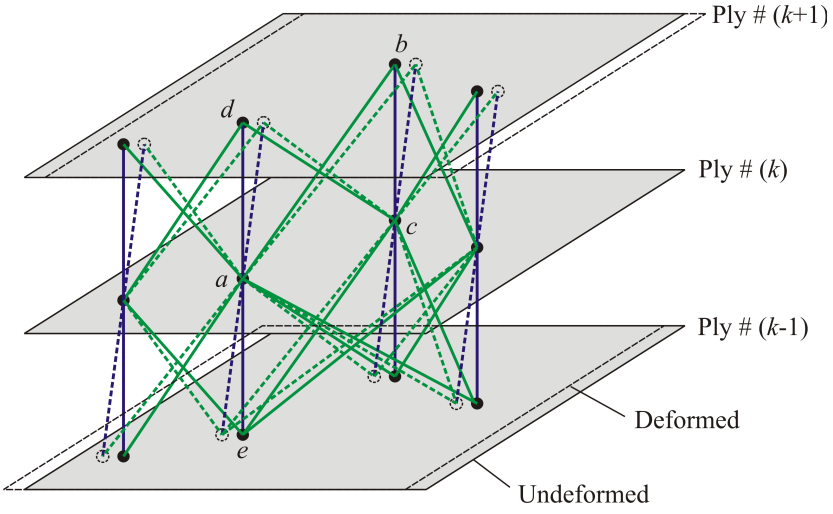

Figure C.6. Deformation of interlayer and shear bonds between neighboring plies (only some of the interactions are depicted explicitly for clarity).

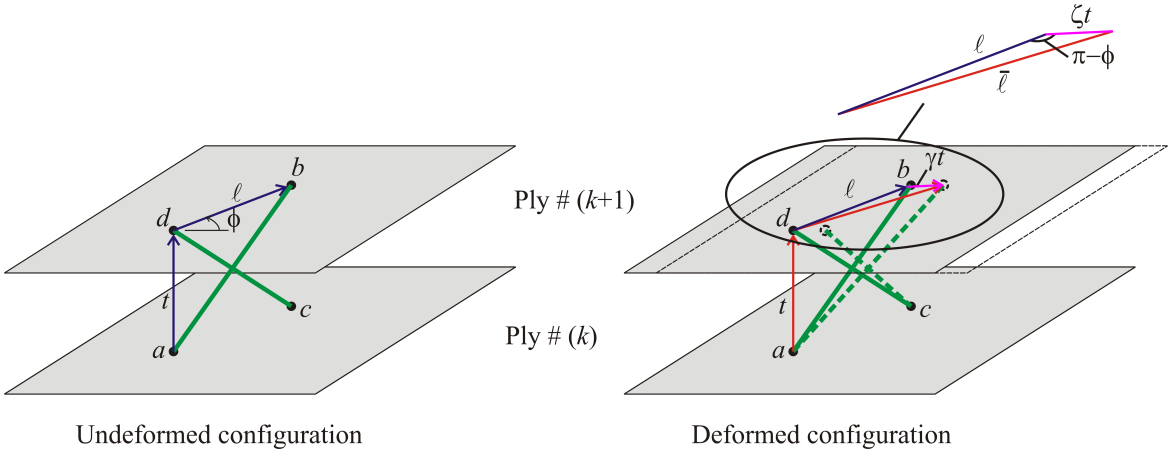

Figure C.7. Shear bonds between material points b and a, and between material points d and c, in both undeformed and deformed configurations.

For the triangle depicted in Figure C.7, by utilizing the law of cosines, the length of the radial component of the deformed bond vector, $\bar{\ell}$, can be written in terms of the length of the radial component of the original bond vector, ℓ, and magnitude of displacement vector, ζt, as

$$\bar{\ell}^2 = \ell^2 + (\zeta t)^2 - 2\ell\zeta t \cos(\pi - \theta). \tag{C.10}$$

After substituting (C.10) in (C.9b), the deformed bond length can be rewritten as

$$|\boldsymbol{\xi}_{ba} + \boldsymbol{\eta}_{ba}| = \sqrt{\ell^2 + t^2 + 2\ell\zeta t \cos(\theta)}. \tag{C.11}$$

In deriving (C.11), the $(\zeta t)^2$ term is neglected with respect to t^2 because ζ is much less than unity. The square root term on the right-hand side of (C.11) can be further simplified by using the square root approximation

$$\sqrt{N^2+d} = N + \frac{d}{2N}, \tag{C.12}$$

where $d \ll N$. Therefore, the deformed bond length expression given in (C.11) can be rewritten as

$$|\boldsymbol{\xi}_{ba} + \boldsymbol{\eta}_{ba}| = \sqrt{\ell^2+t^2} + \frac{\ell\zeta t\cos(\theta)}{\sqrt{\ell^2+t^2}}. \tag{C.13}$$

The original and deformed bond lengths between material points d and c can be computed similarly as

$$|\boldsymbol{\xi}_{dc}| = \sqrt{\ell^2+t^2}, \tag{C.14a}$$

$$|\boldsymbol{\xi}_{dc} + \boldsymbol{\eta}_{dc}| = \sqrt{\ell^2+t^2} - \frac{\ell\zeta t\cos(\theta)}{\sqrt{\ell^2+t^2}}. \tag{C.14b}$$

Therefore, the shear angle for this loading condition can be computed using (C.4) as

$$\varphi = \frac{\ell\zeta\cos(\theta)}{\sqrt{\ell^2+t^2}}. \tag{C.15}$$

After substituting the shear angle expression given in (C.15) to the strain energy density expression given in (C.1), performing the integration results in

$$U_{\mathrm{PD}} = \left\{\frac{\pi c_s t}{4}\left(\delta^2 + t^2\ln\frac{t^2}{t^2+\delta^2}\right)\right\}\zeta^2. \tag{C.16}$$

The corresponding strain energy density based on classical continuum mechanics can be computed as

$$U_{\mathrm{CCM}} = \tfrac{1}{2}G_m\zeta^2. \tag{C.17}$$

After equating the strain energy densities calculated from PD theory and classical continuum mechanics, that is, (C.16) and (C.17), leads to the explicit form of the shear bond constant in terms of the shear modulus of the matrix material, G_m,

$$c_{i\mathrm{S}} = \frac{2G_m}{\pi t}\frac{1}{\left(\delta^2 + t^2\ln\left(\frac{t^2}{\delta^2+t^2}\right)\right)}. \tag{C.18}$$

Appendix D: Critical stretch values for bond constants

The critical stretch value for fiber and matrix bonds can be obtained by performing various experiments as explained in [Oterkus et al. 2012]. In this study, for simplicity, the matrix bond constant is evaluated by using the critical stretch expression given by (12) for an isotropic matrix material, that is, epoxy. The derivation of this critical stretch expression is given by [Silling and Askari 2005]. The elastic, bulk, and shear moduli of the epoxy material are specified as $E_m = 3.792\,\mathrm{GPa}$, $\kappa_m = 3.792\,\mathrm{GPa}$, and $G_m = 1.422\,\mathrm{GPa}$, respectively. It has a critical energy release rate of $G_{\mathrm{IC}} = 2.37\times10^{-3}$ MPa-m. Therefore,

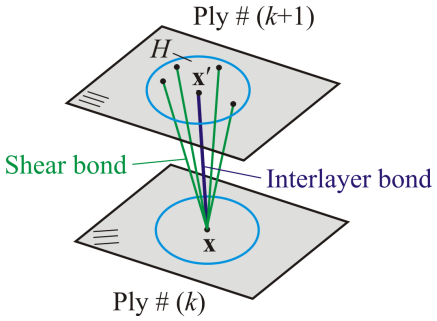

Figure D.8. Interlayer and shear bonds between material point $\boldsymbol{x}$ and other material points located at the $(k+1)$-th ply.

the critical stretch expression of the matrix bond for a horizon value of $\delta = 1.92 \times 10^{-3}$ m can be computed as

$$s_{\text{mt}} = \sqrt{\frac{5G_{\text{IC}}}{9\kappa_m \delta}} = 0.0135. \tag{D.1}$$

The critical stretch for the interlayer bond, $s_{i\text{n}}$, can be computed by equating the energy required to break an interlayer bond between material point $\boldsymbol{x}$ located at the k-th ply and material point $\boldsymbol{x}'$ located at the $(k+1)$-th ply, shown in Figure D.8, to the mode-I critical energy release rate of the material G_{IC} as

$$t\left(\frac{c_{i\text{n}} s_{i\text{n}}^2 t}{2}\right)\overline{V} = G_{\text{IC}}, \tag{D.2}$$

where t and $\overline{V}$ represent the thickness of the ply and the volume of the material point, $\boldsymbol{x}'$, respectively.

Using the relation given by (D.2) in conjunction with the bond constant expression given by $(27)_1$ results in the critical stretch expression for the interlayer bond as

$$s_{i\text{n}} = \sqrt{\frac{2G_{\text{IC}}}{t E_m}}. \tag{D.3}$$

This critical stretch value for epoxy material with a ply thickness of $t = 1.651 \times 10^{-4}$ m is computed as $s_{i\text{n}} = 0.087$.

As opposed to interlayer bonds, multiple shear bonds exist between the material point $\boldsymbol{x}$ and other material points in the $(k+1)$-th ply, as shown in Figure D.8. The failure of these shear bonds corresponds to a mode-II type of failure. Therefore, the energy required to break all of these shear bonds can be equated to the mode-II critical energy release rate of the material, G_{IIC}, as

$$t\int_H \frac{c_{i\text{s}}\varphi_c^2}{2}\, dH = G_{\text{IIC}}, \tag{D.4}$$

where φ_c is the critical shear angle. This equation is rewritten, after splitting the domain of integration, as

$$t\left(t\frac{c_{i\text{s}}\varphi_c^2}{2}\int_0^{\delta} \ell\, d\ell \int_0^{2\pi} d\phi\right) = G_{\text{II}}. \tag{D.5}$$

Performing the integrations results in the critical shear angle expression:

$$\varphi_c = \sqrt{\frac{G_{\mathrm{IIC}}}{tG_m}}. \tag{D.6}$$

As explained in [Araki et al. 2005], the value of the mode-II critical energy release rate of the material, G_{IIC}, is dependent on the postcuring temperature of epoxy. Therefore, it is assumed that G_{IIC} is equal to $\frac{3}{4}G_{\mathrm{IC}}$, which results in the critical shear angle, φ_c, being equal to the critical stretch, $s_{i\mathrm{n}}$, that is, $\varphi_c = s_{i\mathrm{n}} = 0.087$.

References

[Araki et al. 2005] W. Araki, K. Nemoto, T. Adachi, and A. Yamaji, "Fracture toughness for mixed mode I/II epoxy resin", *Acta Mater.* **53**:3 (2005), 869–875.

[Askari et al. 2006] E. Askari, J. Xu, and S. Silling, "Peridynamic analysis of damage and failure in composites", in *44th AIAA/ASME/ASCE/AHS/ASC Aerospace Sciences Meeting and Exhibit* (Reno, NV, 2006), AIAA, Reston, VA, 2006. Paper #2006-88.

[Bogert et al. 2006] P. B. Bogert, A. Satyanarayana, and P. B. Chuncu, "Comparison of damage path predictions for composite laminates by explicit and standard finite element analysis tools", in *47th AIAA/ASME/ASCE/AHS/ASC Structures, Structural Dynamics, and Materials Conference* (Newport, RI, 2006), AIAA, Reston, VA, 2006. Paper #2006-1750.

[Colavito et al. 2007a] K. W. Colavito, B. Kilic, E. Celik, E. Madenci, E. Askari, and S. Silling, "Effect of nanoparticles on stiffness and impact strength of composites", in *48th AIAA/ASME/ASCE/AHS/ASC Structures, Structural Dynamics, and Materials Conference* (Honolulu, 2007), AIAA, Reston, VA, 2007. Paper #2007-2021.

[Colavito et al. 2007b] K. W. Colavito, B. Kilic, E. Celik, E. Madenci, E. Askari, and S. Silling, "Effect of void content on stiffness and strength of composites by peridynamic analysis and static indentation test", in *48th AIAA/ASME/ASCE/AHS/ASC Structures, Structural Dynamics, and Materials Conference* (Honolulu, 2007), AIAA, Reston, VA, 2007. Paper #2007-2251.

[Gerstle et al. 2005] W. Gerstle, N. Sau, and A. Silling, "Peridynamic modeling of plain and reinforced concrete structures", pp. 54–68 in *18th International Conference on Structural Mechanics in Reactor Technology* (Beijing, 2005), SMiRT **18**, IASMiRT, Raleigh, NC, 2005. Paper #B01-2.

[Green et al. 2007] B. G. Green, M. R. Wisnom, and S. R. Hallet, "An experimental investigation into the tensile strength scaling of notched composites", *Compos. A Appl. Sci. Manuf.* **38**:3 (2007), 867–878.

[Hallett and Wisnom 2006] S. R. Hallett and M. R. Wisnom, "Experimental investigation of progressive damage and the effect of layup in notched tensile tests", *J. Compos. Mater.* **40**:2 (2006), 119–141.

[Kaw 2006] A. K. Kaw, *Mechanics of composite materials*, 2nd ed., CRC Press, Boca Raton, FL, 2006.

[Kilic 2008] B. Kilic, *Peridynamic theory for progressive failure prediction in homogeneous and heterogeneous materials*, Ph.D. thesis, Department of Aerospace and Mechanical Engineering, University of Arizona, Tucson, AZ, 2008.

[Kilic et al. 2009] B. Kilic, A. Agwai, and E. Madenci, "Peridynamic theory for progressive damage prediction in centre-cracked composite laminates", *Compos. Struct.* **90**:2 (2009), 141–151.

[Macek and Silling 2007] R. W. Macek and S. A. Silling, "Peridynamics via finite element analysis", *Finite Elem. Anal. Des.* **43**:15 (2007), 1169–1178.

[Oterkus and Madenci 2012] E. Oterkus and E. Madenci, "Peridynamics based on the principle of virtual work", in *53th AIAA/ASME/ASCE/AHS/ASC Structures, Structural Dynamics, and Materials Conference* (Honolulu, 2012), AIAA, Reston, VA, 2012.

[Oterkus et al. 2010] E. Oterkus, A. Barut, and E. Madenci, "Damage growth prediction from loaded composite fastener holes by using peridynamic theory", in *51st AIAA/ASME/ASCE/AHS/ASC Structures, Structural Dynamics, and Materials Conference* (Orlando, FL, 2010), AIAA, Reston, VA, 2010. Paper #2010-3026.

[Oterkus et al. 2012] E. Oterkus, E. Madenci, O. Weckner, S. Silling, P. Bogert, and A. Tessler, "Combined finite element and peridynamic analyses for predicting failure in a stiffened composite curved panel with a central slot", *Compos. Struct.* **94** (2012), 839–850.

[Satyanarayana et al. 2007] A. Satyanarayana, P. B. Bogert, and P. B. Chuncu, "The effect of delamination on damage path and failure load prediction for notched composite laminates", in *48th AIAA/ASME/ASCE/AHS/ASC Structures, Structural Dynamics, and Materials Conference* (Honolulu, 2007), AIAA, Reston, VA, 2007. Paper #2007-1993.

[Silling 2000] S. A. Silling, "Reformulation of elasticity theory for discontinuities and long-range forces", *J. Mech. Phys. Solids* **48**:1 (2000), 175–209.

[Silling and Askari 2005] S. A. Silling and E. Askari, "A meshfree method based on the peridynamic model of solid mechanics", *Comput. Struct.* **83**:17–18 (2005), 1526–1535.

[Silling et al. 2007] S. A. Silling, M. Epton, O. Weckner, J. Xu, and E. Askari, "Peridynamic states and constitutive modeling", *J. Elasticity* **88**:2 (2007), 151–184.

[Wu 1968] E. M. Wu, "Fracture mechanics of anisotropic plates", pp. 20–43 in *Composite Materials Workshop* (St. Louis, MO, 1967), edited by S. W. Tsai et al., Progress in Materials Science **1**, Technomic, Stamford, CT, 1968.

[Xu et al. 2007] J. Xu, A. Askari, O. Weckner, H. Razi, and S. Silling, "Damage and failure analysis of composite laminates under biaxial loads", in *48th AIAA/ASME/ASCE/AHS/ASC Structures, Structural Dynamics, and Materials Conference* (Honolulu, 2007), AIAA, Reston, VA, 2007. Paper #2007-2315.

[Xu et al. 2008] J. Xu, A. Askari, O. Weckner, and S. Silling, "Peridynamic analysis of impact damage in composite laminates", *J. Aerosp. Eng.* (*ASCE*) **21**:3 (2008), 187–194.

Received 2 Dec 2010. Revised 13 Aug 2011. Accepted 4 Sep 2011.

ERKAN OTERKUS: erkan.oterkus@strath.ac.uk
Department of Naval Architecture and Marine Engineering, University of Strathclyde, Henry Dyer Building, 100 Montrose street, Glasgow G4 0LZ, United Kingdom

ERDOGAN MADENCI: madenci@email.arizona.edu
Department of Aerospace and Mechanical Engineering, The University of Arizona, Tucson, AZ 85721-0119, United States

JOURNAL OF MECHANICS OF MATERIALS AND STRUCTURES

jomms.net

Founded by Charles R. Steele and Marie-Louise Steele

See http://jomms.net for submission guidelines.

JoMMS (ISSN 1559-3959) is published in 10 issues a year. The subscription price for 2012 is US $555/year for the electronic version, and $735/year (+$60 shipping outside the US) for print and electronic. Subscriptions, requests for back issues, and changes of address should be sent to Mathematical Sciences Publishers, Department of Mathematics, University of California, Berkeley, CA 94720–3840.

JoMMS peer-review and production is managed by EditFLOW® from Mathematical Sciences Publishers.

PUBLISHED BY
mathematical sciences publishers
http://msp.org/

A NON-PROFIT CORPORATION

Typeset in LaTeX

Journal of Mechanics of Materials and Structures

Volume 7, No. 1 January 2012

1559-3959(2012)7:1;1-D